Regional-Scale Lithospheric Recycling on Venus via Peel-Back Delamination

Andrea Adams[1], Dave Stegman[2], Suzanne E Smrekar[3], and Paul James Tackley[4]

[1]Scripps Institution of Oceanography, University of California San Diego
[2]Scripps Institution of Oceanography
[3]Jet Propulsion Laboratory
[4]ETH Zurich

November 22, 2022

Abstract

We currently have a limited understanding of the tectonic framework that governs Venus. Schubert and Sandwell (1995) identified over 10,000 km of possible subduction sites at both coronae and chasmata rift zones. Previous numerical and experimental studies have shown the viability of regional-scale lithospheric recycling via plume-lithosphere interactions at coronae, yet little work has been done to study the possibility of resurfacing initiated at Venusian rift zones. We created 2D numerical models to test if and how regional-scale resurfacing could be initiated at a lateral lithospheric discontinuity. We observed several instances of peel-back delamination - a form of lithospheric recycling in which the dense lithospheric mantle decouples and peels away from the weak, initially 30 km-thick crust, leaving behind a hot, thinned layer of crust at the surface. Delamination initiation is driven by the negative buoyancy of the lithospheric mantle and is resisted by the coupling of the plate across the Moho, the significant positive buoyancy of the crust arising from a range of crustal densities, and the viscous strength of the plate. Initial plate bending promotes yielding and weakening in the crust, which is crucial to allow decoupling of the crust and lithospheric mantle. When there is sufficient excess negative buoyancy in the lithospheric mantle, both positively and negatively buoyant plates may undergo delamination. Following a delamination event, the emplacement of hot, buoyant asthenosphere beneath the crust may have consequences for regional-scale volcanism and local tectonic deformation on Venus within the context of the regional equilibrium resurfacing hypothesis.

Regional-Scale Lithospheric Recycling on Venus via Peel-Back Delamination

A. C. Adams[1], D. R. Stegman[1], S. E. Smrekar[2], P. J. Tackley[3]

[1]Institute of Geophysics and Planetary Physics, Scripps Institution of Oceanography, University of California, San Diego, CA, USA

[2]Jet Propulsion Laboratory, California Institute of Technology, Pasadena, CA, USA

[3]Institute of Geophysics, Department of Earth Sciences, ETH Zürich, Zürich, Switzerland

Key Points:

- Dense lithospheric mantle on Venus can decouple from crust at the surface and be recycled into the interior
- A regime diagram provides the conditions when peel-back delamination is favored over stagnant-lid despite having net positive plate buoyancy
- Peel-back delamination may be a source of tectonic/volcanic resurfacing within the framework of regional equilibrium resurfacing

Corresponding author: Andrea Adams, aca009@ucsd.edu

Abstract

We currently have a limited understanding of the tectonic framework that governs Venus. Schubert and Sandwell (1995) identified over 10,000 km of possible subduction sites at both coronae and chasmata rift zones. Previous numerical and experimental studies have shown the viability of regional-scale lithospheric recycling via plume-lithosphere interactions at coronae, yet little work has been done to study the possibility of resurfacing initiated at Venusian rift zones. We created 2D numerical models to test if and how regional-scale resurfacing could be initiated at a lateral lithospheric discontinuity. We observed several instances of peel-back delamination - a form of lithospheric recycling in which the dense lithospheric mantle decouples and peels away from the weak, initially 30 km-thick crust, leaving behind a hot, thinned layer of crust at the surface. Delamination initiation is driven by the negative buoyancy of the lithospheric mantle and is resisted by the coupling of the plate across the Moho, the significant positive buoyancy of the crust arising from a range of crustal densities, and the viscous strength of the plate. Initial plate bending promotes yielding and weakening in the crust, which is crucial to allow decoupling of the crust and lithospheric mantle. When there is sufficient excess negative buoyancy in the lithospheric mantle, both positively and negatively buoyant plates may undergo delamination. Following a delamination event, the emplacement of hot, buoyant asthenosphere beneath the crust may have consequences for regional-scale volcanism and local tectonic deformation on Venus within the context of the regional equilibrium resurfacing hypothesis.

1 Introduction

We currently lack an understanding of the global tectonic and convective framework that has governed Venus throughout its evolution. On Earth, resurfacing occurs via plate tectonics, where new crust is formed at mid-ocean ridges and old lithosphere is continuously recycled at subduction zones. Despite being Earth's closest neighbor in the solar system and having similarities in size and composition, Venus shows no evidence of Earth-like plate tectonics (Phillips & Hansen, 1994; Solomon et al., 1992). Since NASA's Magellan mission in the early 1990s, two key observations related to impact craters have guided our insight into how the surface of Venus may have evolved over time: approx-

imately 975 total craters suggest a relatively young surface age (250-750 Myr) (Feuvre & Wieczorek, 2011; McKinnon et al., 1997; Schaber et al., 1992; Turcotte, 1993) and the crater population has a near spatially random distribution (Phillips et al., 1992; Riedel et al., 2021; Strom et al., 1994). In the decades since Magellan, these observations have divided ideas about Venus' surface evolution into two hypotheses: (1) the catastrophic/episodic resurfacing hypothesis and (2) the equilibrium resurfacing hypothesis.

The catastrophic resurfacing (CR) model describes a tectonic regime where the cooling and thickening of Venus' lithosphere is interrupted by at least one, but perhaps multiple global-scale overturns over the last 4.5 billion years (Parmentier & Hess, 1992; Turcotte, 1993, 1995; Turcotte et al., 1999). These events are thought to occur over relatively short geologic timescales (<100 Myr) and are followed by a period of resurfacing (Namiki & Solomon, 1994; Strom et al., 1994). This theory rose in popularity because the post-overturn uniform surface age is a simple explanation for the spatially random crater distribution on Venus. The young surface age implies that the most recent overturn event happened in the last 250-750 Myr, and the CR hypothesis attributes the mostly unmodified crater population to low levels of tectonic or volcanic activity during the following quiescent period (Herrick, 1994; Schaber et al., 1992). Convection models from previous studies support the CR hypothesis by producing cyclic global overturn events under certain conditions (Armann & Tackley, 2012; Crameri & Tackley, 2016; Moresi & Solomatov, 1998; Reese et al., 1999; Rolf et al., 2018; Weller & Kiefer, 2020; Uppalapati et al., 2020).

Despite being compatible with first-order cratering constraints, the CR model is not unequivocally supported by all models and observations. The offset between the center of mass and center of figure (CM-CF) of Venus is a measurable quantity that can signal large-scale density anomalies in a planet's surface (topography) and interior (thermal anomalies). King (2018) analyzed the immediate and long-term effects of one or more global overturns on the calculated CM-CF offset in models of Venus. The calculated offsets were significantly larger than the the observed CM-CF offset, indicating the observed offset is incompatible with a global resurfacing event (King, 2018). Furthermore, the CR hypothesis can be rejected because a uniform surface age contradicts observations that different stages of impact crater degradation are associated with different geological regions on Venus (Basilevsky & Head, 2002; Herrick & Rumpf, 2011; Izenberg et al., 1994). Combined with the association between crater density and geology, the three average model

surface age (AMSA) provinces dividing the surface of Venus into relative ages (old, intermediate, and young) (Hansen & Young, 2007; Phillips & Izenberg, 1995), point toward a more complex resurfacing history.

The competing idea to explain Venus's unique style of resurfacing is the regional equilibrium resurfacing (RER) hypothesis. It suggests Venus' crater population is a balance between steady-state crater formation and the removal of craters by tectonic or volcanic processes occurring at different rates regionally (Phillips et al., 1991, 1992). Although some early statistical analyses could not reconcile the observed crater population with frequent, smaller resurfacing events (Bullock et al., 1993; Strom et al., 1994), more recent Monte Carlo experiments found that the uniform crater distribution and number of modified craters can be explained by regional equilibrium resurfacing (Bjonnes et al., 2012; O'Rourke et al., 2014). The RER model is also compatible with both the observed CM-CF offset for Venus (King, 2018) as well as the association with crater population and geology (Phillips & Izenberg, 1995). The RER hypothesis is further supported by evidence of regional-scale volcanic activity from thermal emissivity anomalies observed at volcanoes (Shalygin et al., 2012) and chasma rift zones (Shalygin et al., 2015). Surface emissivity data indicating a lack of chemical weathering at coronae and volcanoes over plume-associated topographic rises also signify geologically-recent volcanism on Venus (Smrekar et al., 2010).

In addition to volcanic mechanisms of resurfacing, there is evidence that tectonic processes may also drive regional-scale resurfacing events. Sandwell and Schubert (1992) observed that trench-outer rise topography and lithospheric flexure across several of Venus' largest coronae are comparable to various arcuate subduction zones on Earth (Sandwell & Schubert, 1992). This is interpreted as evidence for retrograde subduction which may have initiated due to interactions between the lithosphere and a rising mantle plume. The viability of plume-induced subduction at Venusian coronae has since been studied in both numerical (Gülcher et al., 2020) and laboratory experiments (Davaille et al., 2017) and is the favored model for regional-scale subduction on Venus - in part because the plume provides a mechanism to weaken and break the lithosphere. Melt weakening (Gülcher et al., 2020) and loading due to surface volcanism (Sandwell & Schubert, 1992) may cause the lithosphere to break and its edges to sink and migrate radially outward. Plume-induced subduction may be ongoing at present, as evidenced by anomalously-high thermal emis-

sivity at Quetzalpetlatl corona indicating geologically-recent volcanism (Davaille et al., 2017).

Plume-lithosphere interactions are a mechanism to induce weakness in the lithosphere and facilitate subduction initiation, but subduction itself is primarily driven by the negative buoyancy of the plate. For Venus, this could be complicated. Large regional variations (and uncertainties) in crust and lithosphere thickness (Anderson & Smrekar, 2006; James et al., 2013) and potentially warmer mantle temperatures with higher degrees of melting and crust formation affect the net buoyancy of the lithosphere and its ability to subduct. In order to better understand the viability of regional-scale tectonic resurfacing, it is important to constrain a range of conditions for which lithospheric recycling may occur on Venus without the added complexities of plume-lithosphere interactions. In addition to coronae, thousands of kilometers of chasmata (Dali and Diana chasmata, Hecate Chasma, Parga Chasma, etc.), or rift zones, are proposed to be possible sites of subduction on Venus (Sandwell & Schubert, 1992; Schubert & Sandwell, 1995). Here, we present 2D numerical models of a simplified Venusian rift zone over a range of crust and mantle conditions to identify if and how regional-scale lithospheric recycling can occur without assistance from mantle plume interactions.

2 Methods

2.1 Model Setup

We performed a series of numerical experiments using StagYY, a finite-volume code which models solid-state mantle convection by solving the conservation of mass, momentum, and energy equations on a staggered grid (Tackley, 2008). We consider viscous flow of an infinite Prandtl number fluid and assume an incompressible mantle using the Boussinesq approximation. Composition is tracked using over 13.6 million (13694800) tracer particles in a 2048x512 resolution grid space. All visualization was performed using StagLab (Crameri, 2018).

2.2 Initial Condition

The model geometry is a two-dimensional 180° spherical annulus (Hernlund & Tackley, 2008). The initial condition consists of a lithosphere with a single discontinuity where a 250 km-wide gap separates two edges of the lithospheric mantle (Fig. 1). The gap is

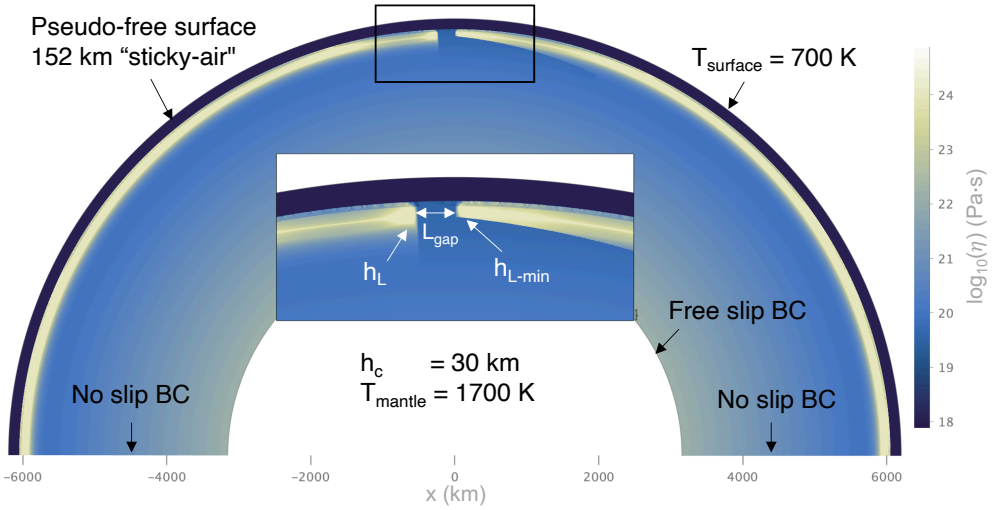

Figure 1. Viscosity field of initial model setup. A gap (L_{gap} = 250 km) separates two plate edges with thicknesses h_L = [200, 250, or 300] km (left) and h_{L-min} = 100 km (right). The lithosphere with thickness h_{L-min} gradually thickens to be thickness h_L. The gap represents a simplified rift zone or an area having undergone previous magmatic weakening. The model setup is designed to study buoyancy-driven lithospheric recycling events in the absence of an imposed velocity field or slab perturbation as to be more representative of Venus.

filled with relatively warm asthenospheric material. The gap is a simplified representation of a rift zone or an area where a previous thermal upwelling left behind an area of magmatically-weakened lithosphere. Rift widths are locally similar to the model gap between plates. For example, the 10,000 km long fracture zone of Parga Chasma varies from 90-590 km; the trough is 60-230 km wide and 0.5-2 km deep (Martin et al., 2007). A 30 km-thick layer of basaltic crust (h_c) covers the entire domain including the gap. The plate to the left of the gap is uniformly thick (h_L = [200, 250, 300] km) and covers an upper range of lithosphere thicknesses that may be present on Venus (Anderson & Smrekar, 2006). The plate to the right of the gap is thinned at its edge (constant h_{L-min} = 100 km) and gradually thickens to h_L. The asymmetry in lithospheric thickness across the gap may reflect cases of observed asymmetry across Venusian chasmata (Schubert & Sandwell, 1995). We use a mantle potential temperature of 1700 K (Nimmo & McKenzie, 1997; Shellnutt, 2016) and define lithosphere thickness by the 1600 K isotherm. There is no initial velocity-field perturbation or pre-existing plate bending to assist the initiation of plate motion.

2.3 Boundary Conditions

All models employ a pseudo-free-surface upper boundary condition with 152 km of "sticky-air" which allows for the development of realistic topography and is known to influence lithosphere dynamics (Crameri et al., 2012). The surface temperature is defined by a 700 K isothermal boundary. We use a free-slip lower boundary and no-slip sidewall boundary conditions. The no-slip sidewall boundaries simulate the resistance of the surface to slab pull during potential lithospheric recycling events, which may best represent an effectively single-plate planet such as Venus. The sidewall boundaries are sufficiently far from the gap so there is no interference with local mantle flow.

2.4 Viscosity

Diffusion creep and plastic failure are assumed to be the only deformation mechanisms. Temperature and pressure-dependent viscosity is defined by the Arrhenius law:

$$\eta(T,p) = \eta_0 \cdot exp\left[\frac{E_a + (1-z)V_a}{T} - \frac{E_a}{T_0}\right] \tag{1}$$

where E_a and V_a are the activation energy and volume, respectively, and the reference viscosity, η_0, is 10^{20} Pa·s at zero pressure and 1600 K. An activation energy of 240 kJ/mol was chosen corresponding to a wet olivine rheology. Although the model has an incompressible mantle, we included an amount of viscosity increase with depth that is equivalent to that of a compressible mantle. We estimated that the net effect of pressure and temperature dependence in a compressible mantle would cause a viscosity increase of approximately three orders of magnitude, and therefore adopted a value of 50% V_a which provides an comparable increase over depth. Viscosity variations in the mantle were restricted to six orders of magnitude with a maximum viscosity of 10^{25} Pa·s and a minimum viscosity of 10^{19} Pa·s. The viscosity of the sticky-air was 10^{18} Pa·s. The maximum viscosity of the lithosphere was controlled separately and varied between three values spanning two orders of magnitude, $\eta_{max} = [10^{23}, 10^{24}, 10^{25}]$ Pa·s.

2.5 Yield Strength

Plasticity is implemented using the Drucker-Prager criterion based on Byerlee's law to calculate the pressure-dependent brittle yield stress

$$\tau_{y,brittle} = C + p\mu \tag{2}$$

with cohesion, C, confining pressure, p, and friction coefficient, μ. The models described here all use a surface cohesion of 10 MPa and a friction coefficient of 0.25. The effective yield stress τ_y is then calculated as the minimum between $\tau_{y,brittle}$ and a constant maximum yield stress

$$\tau_y = min[\tau_{y,brittle}, \tau_{max}] \tag{3}$$

which effectively limits the yield stress to a maximum value of τ_{max} at higher pressure and depth. When stress levels exceed the yield stress, the material strength is reduced by converting the viscosity into an effective viscosity

$$\eta \begin{cases} \eta = \frac{\tau_\Pi}{2\dot{\epsilon}_\Pi} & \text{for} \quad \tau < \tau_{yield} \\ \eta_{eff} = \frac{\tau_{yield}}{2\dot{\epsilon}_\Pi} & \text{for} \quad \tau \geq \tau_{yield} \end{cases} \tag{4}$$

When the yield stress is exceeded, stresses in the lithosphere are redistributed to accommodate the decrease in material strength. While previous models of global overturns on Venus use maximum yield stresses (τ_{max}) near 100 MPa (Armann & Tackley, 2012), we chose to employ a maximum yield stress of 500 MPa. This will give a yield stress (τ_y) with depth that is stronger throughout the depth of the lithosphere (Fig. 2). The crust on Venus is suspected to be relatively weak and decoupled from the underlying mantle (Arkani-Hamed, 1993; Azuma et al., 2014; Buck, 1992; Ghail, 2015) and in our models is represented by a material with uniform strength (cohesion of 10 MPa and friction coefficient approximately zero) which readily yields to tectonic forces (Crameri & Tackley, 2016).

2.6 Phase Transitions

Tracer particles are used to track compositions within the olivine and basalt/garnet systems. Compositional phase transitions were implemented as depth-dependent density contrasts within the two systems relative to the reference density ($\rho_0 = 3300$ kg/m^3). Several Earth-like phase changes were included with depths adjusted to Venus's lower gravity (Fig. 3) (Ogawa & Yanagisawa, 2014).

At cooler temperatures inside the subducting slab, the postspinel phase boundary in the olivine system is deflected to deeper depths. Estimates of the value of the postspinel Clapyeron slope, $\gamma_{\rm psp}$, range from -0.2 to -3.0 MPa/K (Akaogi & Ito, 1993; Fei et al., 2004; Irifune et al., 1998; Katsura et al., 2003), where more recent estimates fall closer to zero (Fukao et al., 2009) (see references therein). It is also reported that the effect of

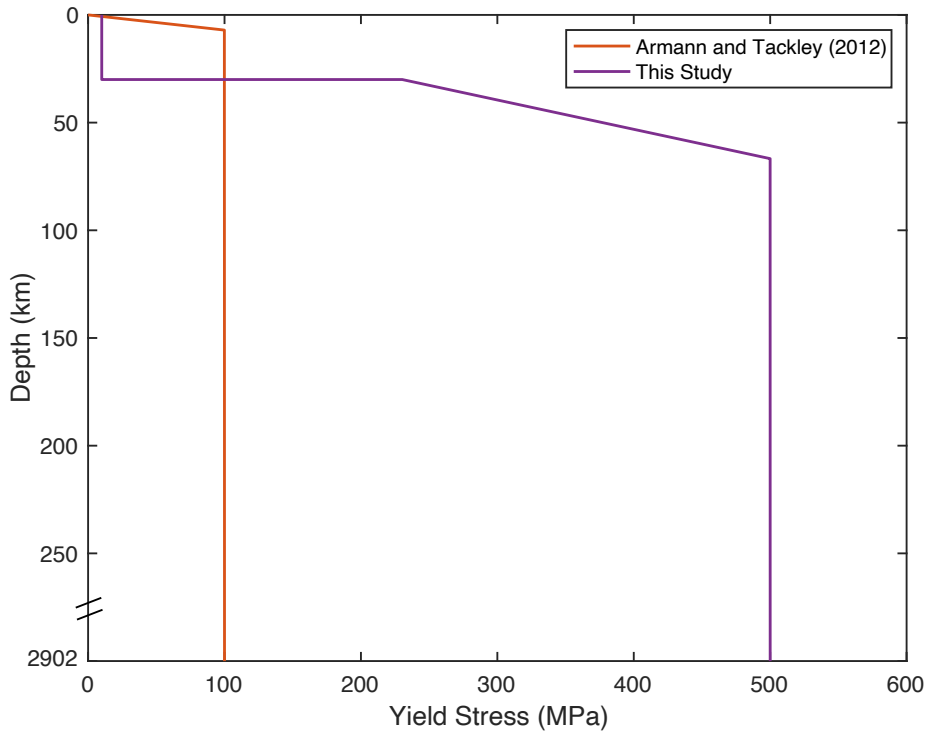

Figure 2. Depth vs yield stress (τ_y) throughout the depth of the mantle. Armann and Tackley (2012) observed global overturns when the maximum yield stress (τ_{max}) was 100 MPa. Our models employ weak crust at the surface and a higher maximum yield stress of 500 MPa through the majority of the lithosphere.

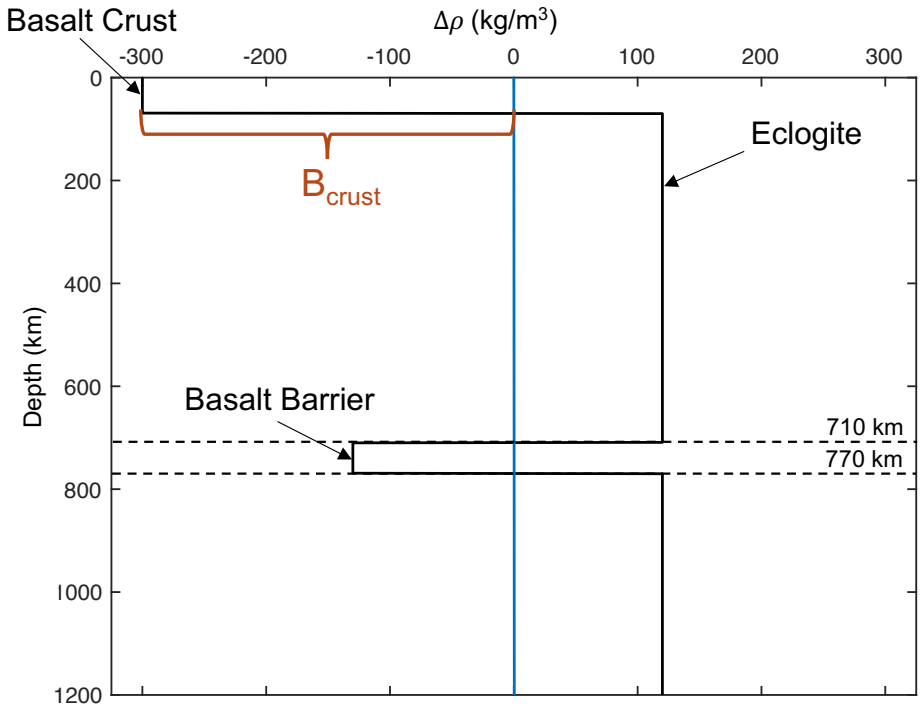

Figure 3. Relative compositional density contrast between basalt-garnet system and olivine system through the depth of the mantle. At the surface, basaltic crust is positively buoyant compared to the reference density (blue line) with $\Delta\rho_c = B_{crust}$ kg/m^3 (variable). Eclogite forms and becomes denser than the reference mantle ($\Delta\rho_{ec}$ = 120 kg/m^3) at 70 km depth. The "basalt barrier" results in a region of positive buoyancy ($\Delta\rho_{bb}$ = -130 kg/m^3) in the basalt-garnet system between 710 and 770 km depth. Adapted from Ogawa and Yanagisawa (2014).

the negative Clapyeron slope is stronger in 2D models than in 3D (Ogawa & Yanagisawa, 2014). A larger Clapyeron slope will deflect the phase boundary to deeper depths and result in a larger region of positive buoyancy within the slab; conversely, a smaller Clapeyron slope may only weakly deflect the postspinel phase boundary. Our models use a value of γ_{psp} = -1.0 MPa/K in order to understand, but not overstate its effect.

At 70 km depth, the positively buoyant crust ($\Delta\rho = B_{crust}$ kg/m^3) transforms into denser eclogite ($\Delta\rho_{ec}$ = 120 kg/m^3). Between 710 and 770 km, the gradual transition of the garnet-bridgmanite transition results in a region of positive buoyancy ($\Delta\rho_{bb}$ = -130 kg/m^3) in the basalt/garnet system relative to bridgmanite. This is referred to as the garnet trap, or basalt barrier (Davies, 2008), and it coincides with the positively buoyant region within the slab that arises due to deflection of the postspinel boundary. Thus, there are two separate sources of positive buoyancy within the down-going plate beginning at 710 km depth, which combined have the potential to inhibit slab sinking. Below the garnet trap, the density contrast of the basalt-garnet system returns to $\Delta\rho$ = 120 kg/m^3.

2.7 Crust Density

The positive compositional buoyancy of the crust counteracts some of the negative buoyancy of the lithosphere, both of which determine the net buoyancy of the plate. In order to explore the effect of crustal buoyancy, we specified the compositional density contrast, $B_{crust} = \rho_{0,crust}$ - ρ_0, which was prescribed to all crust particles. An average crust thickness of 30 km (James et al., 2013) was held constant in order to isolate the effects of net crust buoyancy from the effects of variable crust thickness. We vary B_{crust} = [-175, -265, -300, -350, -400] kg/m^3 (Fig. 3). The lowest density contrast, B_{crust} = -175 kg/m^3, represents the compositional density contrast between olivine and pyroxene-garnet used by Armann and Tackley (2012) in models of global overturns; the highest density contrast, B_{crust} = -400 kg/m^3, represents the expected density contrast for an Earth-like basaltic crust with ρ_{crust}=2900 kg/m^3. Ogawa and Yanagisawa (2014) predict B_{crust} to be -300 kg/m^3 for crust and mantle compositions of $A_{0.1}B_{0.9}$ and $A_{0.64}B_{0.36}$, respectively, where A is harzburgite and B is garnet and pyroxene (Ogawa & Yanagisawa, 2014). In addition to compositional density, we consider thermal effects on density. The crust covering the gap is warmer, and therefore less dense than the crust covering the plate. A minimum crust thickness of 15 km has been enforced over the entire

Table 1. Parameters common to all models

Parameter	Description	Value
R	Planetary radius	6052 km
R_{cmb}	Core radius	3150 km
nx	Horizontal cells	2048
nz	Vertical cells	512
g	Gravitational acceleration	8.9 ms^{-2}
ρ_0	Reference density	3300 kgm^{-3}
Cp	Heat capacity at constant pressure	1200.0 J K^{-1}
k	Thermal conductivity	3 $\mathrm{Wm}^{-1}\mathrm{K}^{-1}$
α	Coefficient of thermal expansion	$3 \times 10^{-5}\mathrm{K}^{-1}$
T_s	Surface temperature	700 K
T_m	Mantle potential temperature	1700 K
η_0	Reference viscosity at $T = 1600$ K	$1 \times 10^{20}\mathrm{Pa} \cdot \mathrm{s}$
E_{eta}	Activation energy for wet olivine diffusion	240 kJ/mol
η_{air}	Air layer viscosity	$1 \times 10^{18}\mathrm{Pa} \cdot \mathrm{s}$
h_{air}	Air layer thickness	152 km
h_c	Crustal thickness	30 km
C_{mantle}	Mantle cohesion	10 MPa
μ_{mantle}	Mantle coefficient of friction	0.25
$C_{weak\ crust}$	Weak crust cohesion	10 MPa
$\mu_{weak\ crust}$	Weak crust coefficient of friction	0.001
γ_{710}	Clapeyron slope of postspinel transition	-1.0 MPaK^{-1}

domain to prevent entrapment of sticky-air particles due to the low viscosity contrast between air and mantle material inside the gap.

3 Results

We investigated lithospheric recycling for a suite of 42 numerical models with variable crust density, lithosphere thickness, and maximum viscosity (see Table 2). Each model within the suite was identified as in either (I) a peel-back delamination regime or (II) a stagnant-lid regime. In this section, we discuss the characteristics of the two regimes and the factors affecting their development. Model 23 is referred to as the reference model due to having intermediate values of crustal buoyancy, plate thickness, and maximum viscosity (B_{crust} = -300 kg/m^3, h_L = 250 km, $\eta_{max} = 10^{24}$ Pa·s).

3.1 Tectonic Regimes

3.1.1 Regime I: Peel-Back Delamination

Peel-back delamination is a type of lithospheric recycling where the lithospheric mantle detaches and peels away from the lower crust along the Moho. It differs from roll-

Table 2. Summary of Model Parameters and Outcomes

Model	Crust Density (kg/m^3)	Lithosphere Thickness (km)	Max. Viscosity (Pa·s)	Outcome
1	-175	200	10^{23}	Delamination
2	-175	200	10^{24}	Delamination
3	-175	200	10^{25}	Delamination
4	-175	250	10^{23}	Delamination
5	-175	250	10^{24}	Delamination
6	-175	250	10^{25}	Delamination
7	-175	300	10^{23}	Delamination
8	-175	300	10^{24}	Delamination
9	-175	300	10^{25}	Delamination
10	-265	200	10^{23}	Stagnant-Lid
11	-265	200	10^{24}	Stagnant-Lid
12	-265	200	10^{25}	Stagnant-Lid
13	-265	250	10^{23}	Delamination
14	-265	250	10^{24}	Delamination
15	-265	250	10^{25}	Delamination
16	-265	300	10^{23}	Delamination
17	-265	300	10^{24}	Delamination
18	-265	300	10^{25}	Delamination
19	-300	200	10^{23}	Stagnant-Lid
20	-300	200	10^{24}	Stagnant-Lid
21	-300	200	10^{25}	Stagnant-Lid
22	-300	250	10^{23}	Delamination
23	-300	250	10^{24}	Delamination
24	-300	250	10^{25}	Delamination
25	-300	300	10^{23}	Delamination
26	-300	300	10^{24}	Delamination
27	-300	300	10^{25}	Delamination
28	-350	200	10^{23}	Stagnant-Lid
29	-350	200	10^{24}	Stagnant-Lid
30	-350	200	10^{25}	Stagnant-Lid
31	-350	250	10^{23}	Delamination
32	-350	250	10^{24}	Delamination
33	-350	250	10^{25}	Stagnant-Lid
34	-350	300	10^{23}	Delamination
35	-350	300	10^{24}	Delamination
36	-350	300	10^{25}	Delamination
37	-400	250	10^{23}	Stagnant-Lid
38	-400	250	10^{24}	Stagnant-Lid
39	-400	250	10^{25}	Stagnant-Lid
40	-400	300	10^{23}	Delamination
41	-400	300	10^{24}	Delamination
42	-400	300	10^{25}	Delamination

back subduction because the majority of the basaltic crust remains at the surface as the denser lithospheric mantle sinks. It also differs from the Rayleigh-Taylor lithospheric dripping style of delamination (Houseman & Molnar, 1997; Johnson et al., 2014) because the full depth of the lithospheric mantle is recycled coherently in each event. The following descriptions apply to all observed cases of peel-back delamination.

Delamination initiation is characterized by several distinct stages (Fig. 4). First, the relatively dense sub-crustal lithospheric mantle (SCLM) begins to bend, which induces yielding in the overlying weak crust. As the stress in the crust exceeds its yield strength, the viscosity of the crust is limited to the effective viscosity (eqn. 4), forming a weak layer near the plate edge which facilitates decoupling of the crust and SCLM (Fig. 4A). As the SCLM continues to bend, buoyant asthenosphere from the gap is wedged between the surface and top of the SCLM. A small amount of buoyant crust (approximately 5 km thick) remains attached to the down-going SCLM, while the majority of crust remains at the surface or as part of a crustal root forming at the hinge of the delaminating plate (Fig. 4D). Once the thin layer of crust on the SCLM reaches the eclogite transition at 70 km depth, it becomes dense relative to the underlying mantle. Simultaneously, the weak zone of yielded crust propagates along the Moho accompanying trench retreat (Fig. 4E-F). As more SCLM progressively detaches from the crust, the crustal root at the trench thickens. When the base of the crustal root reaches 70 km depth, thicker layers of crust undergo the eclogite density inversion (Fig. 4H). The thick layers of eclogite add negative buoyancy to the delaminating plate that help sustain sinking. The thinner lithosphere to the right of the gap never undergoes delamination.

After delamination is initiated (Fig. 5A-B), the slab continues to sink until it approaches the postspinel phase transition at 710 km depth (Fig. 5C). Due to the negative Clapeyron slope of the postspinel phase change, the cooler SCLM becomes positively buoyant relative to the surrounding mantle until it reaches sufficient pressure to undergo the phase transition. The tip of the delaminating slab is deflected in response to encountering both the postspinel density inversion and resistance from the radial viscosity increase with depth in the mantle (Fig. 5C). As the negatively buoyant eclogite layer reaches the basalt barrier between 710-770 km depth, it undergoes a separate density inversion making the basaltic material positively buoyant in relation to the surrounding mantle. As a result, slab sinking is inhibited by two distinct sources of positive buoyancy in the down-going plate beginning at 710 km depth (Fig. 6). As the radial viscosity increases

with depth and the slab reaches both density inversions, the plate bends and the slab tip is deflected to shallower mantle depths (Fig. 5D). When the SCLM and crust material eventually sink past the density inversions due to the weight of the slab, they once again become dense relative to the surrounding mantle. Sinking of the bent plate continues until thinning and viscous necking at the slab hinge cause the plate to break off at the surface (Fig. 5E). All delamination models were run until slab break-off occurred.

3.1.2 Regime II: Stagnant-Lid

A total of thirteen models were categorized as stagnant-lid (see Table 2). A stagnant-lid regime is characterized by the absence of lithospheric recycling. The warm mantle inside the gap is cooled due to being surrounded by the colder surface and lithosphere. Over time, the plate edges are smoothed by the growth of the thermal boundary layer. Model runs were ended when the gap was cooled enough to effectively fuse the plate edges together across the gap. In some cases when the maximum viscosity was relatively low ($\eta_{max} = 10^{23}$ Pa·s), the plates that did not undergo recycling contracted and widened the gap. Ultimately, these plates were unable to bend and initiate crust yielding on timescales that would weaken the crust sufficiently for a delamination interface to form. Despite some initial bending of the lithospheric mantle, the absence of a weak zone prevented these plates from delaminating.

3.2 Analysis of Regimes

3.2.1 Radius of Curvature

The radius of curvature of a down-going slab is a useful metric to describe delamination because it is dependent on both the negative buoyancy of the slab and the viscosity ratio between the slab and upper mantle (Petersen et al., 2017; Schellart, 2010). The radius of curvature (R_c) was calculated for each delamination model every 50 model time steps. The radius of curvature calculation was adapted from the version provided in StagLab (Crameri, 2018). A least squares approximation of a circle was fit to the 1100 K isotherm, which defines the core of the slab from a distance of 400 km behind the trench to a depth of 900 km. This range was chosen to exclude the effect of slab tip deflection resulting from the phase transitions in the mid-mantle.

Different stages of delamination evolution were apparent in the calculated R_c plotted over time (Fig. 7). The radius of curvature was largest before delamination is ini-

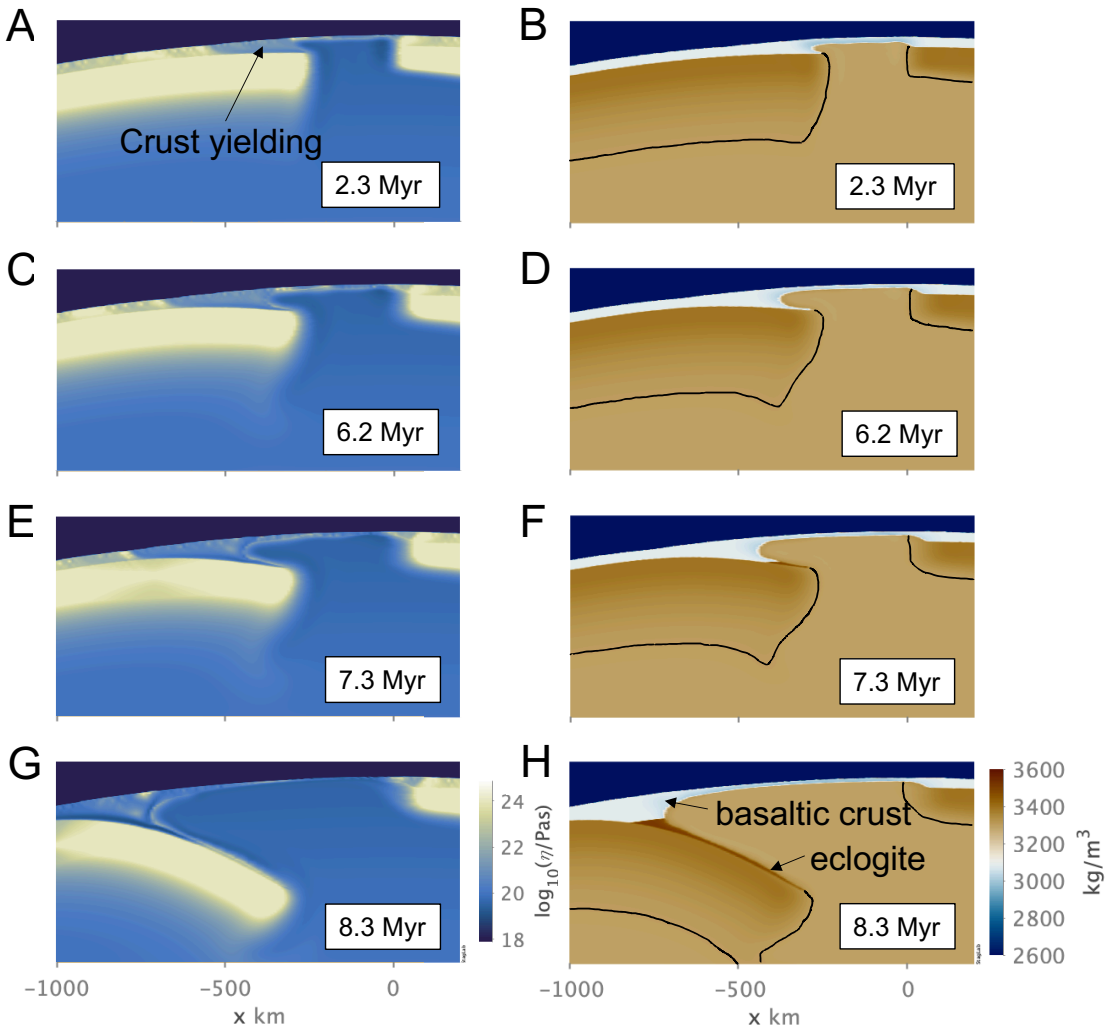

Figure 4. Progression of peel-back delamination initiation shown in the viscosity (left) and density (right) fields of reference model 23 (B_{crust} = -300 kg/m^3, h_L = 250 km, $\eta_{max} = 10^{24}$ Pa·s). A black line is added to the density field to show the boundary of the lithospheric mantle and asthenosphere defined by the 1600 K isotherm. (A-B) Initial bending of the negatively buoyant lithospheric mantle causes weak crust over plate edge to yield and a small weak zone to form. (C-D) The weak zone propagates as the crust is further yielded and buoyant asthenosphere spreads over the delaminating plate edge. Only a thin layer of crust (5 km) is attached to the delaminating plate. (E-F) The crustal root over the delaminating plate hinge thickens and reaches the eclogite transition at 70 km depth, resulting in a density inversion which makes the crust more negatively buoyant than the underlying mantle. (G-H) The delaminating plate continues to detach and peel back from the overlying weak crust layer. Sinking is enhanced by the added negative buoyancy of the eclogitized crust. The thickness of crust attached to the delaminating plate increases as the crustal root deepens and more eclogite is formed. Dark blue layer = sticky-air.

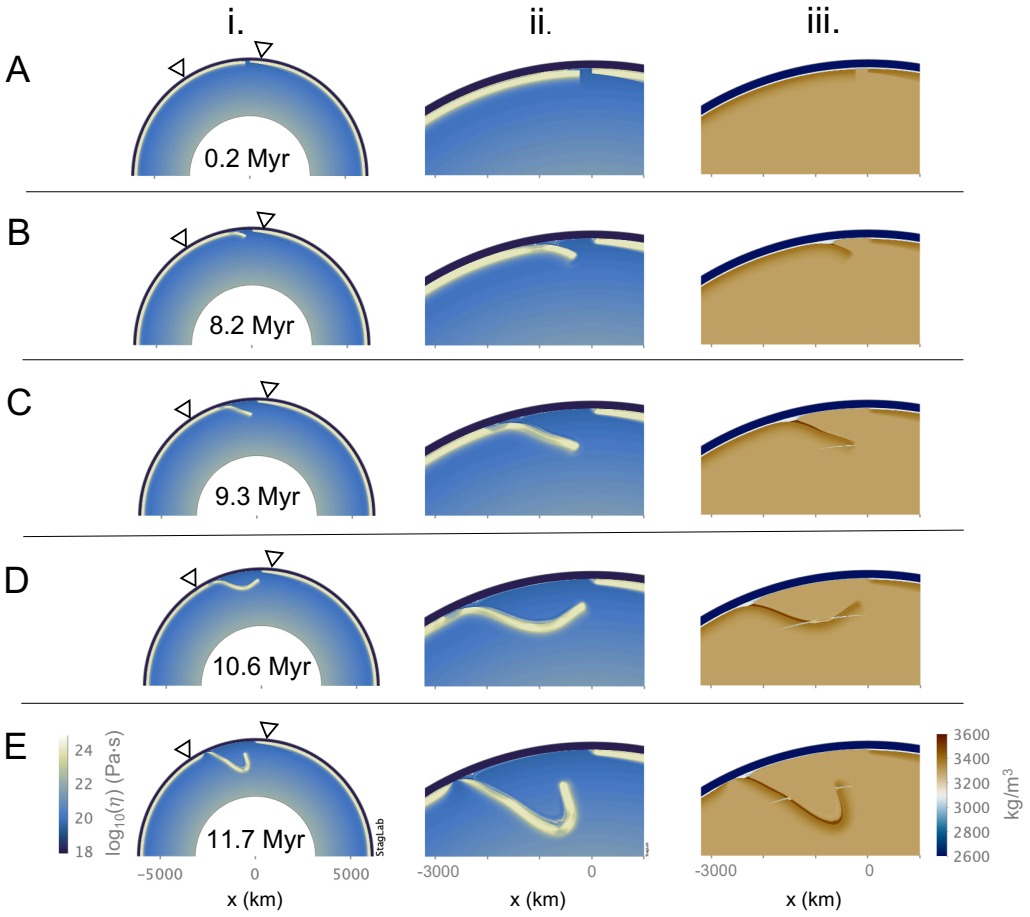

Figure 5. Typical evolution of a peel-back delamination event shown in the (i) full-scale viscosity field, (ii) local viscosity field, and (iii) local density field of reference model 23 (B_{crust} = -300 kg/m^3, h_L = 250 km, $\eta_{max} = 10^{24}$ Pa·s). (A) A 250 km-wide gap separates the thicker plate edge on the left (h_L) from the 100 km plate edge to the right of the gap. (B) The edge of the thicker plate is bent downward due to the negative buoyancy of the lithospheric mantle. A layer of eclogite is formed in the thin layer of crust still attached to the down-going plate. (C) The lithospheric mantle continues to peel-back from the surface and thicker layers of crust are recycled due to eclogitization of the growing crustal root over the delamination hinge. The slab tip encounters the phase transitions near 710 km depth and (D) is deflected upward. (E) The plate necks and thins at the delamination hinge prior to slab break-off at the surface.

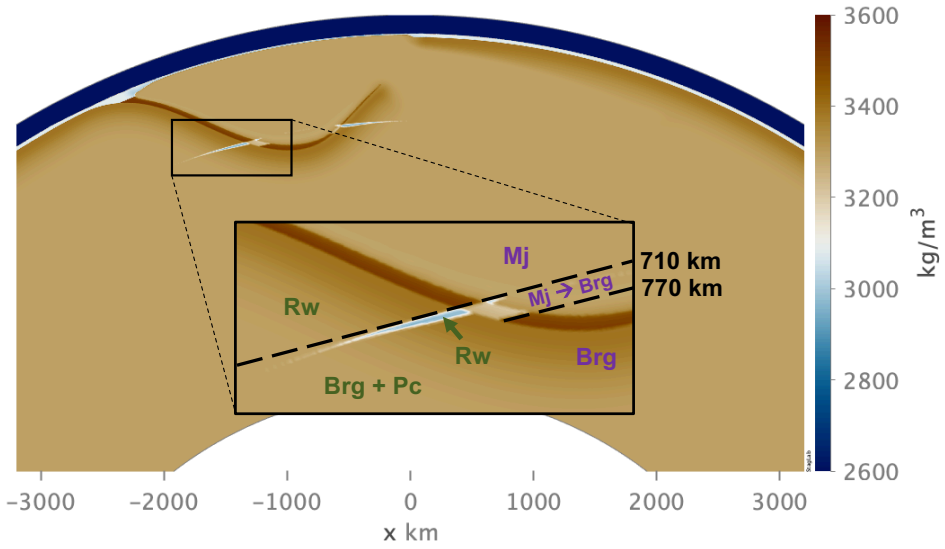

Figure 6. Two separate sources of mid-mantle positive buoyancy within the delaminating slab shown in the density field of the reference model 23. The first is in the olivine system (green text) where the negative Clapeyron slope (-1.0 MPa/K) of the postspinel phase transition deflects the phase boundary to deeper depths within the cold regions of the slab. The transition of ringwoodite (Rw) to bridgmanite (Brg) and periclase (Pc) is delayed, resulting in a thin layer of positive buoyancy within the slab (light blue). The second source of positive buoyancy occurs within the basalt-garnet system (purple text). The basalt barrier is the result of the gradual transition of majorite garnet (Mj) to bridgmanite over 710-770 km depths (light beige).

tiated and oscillated as the plate edge began to founder. Delamination initiation is defined as the point when the plate edge began to bend and sink continuously, which corresponded to the time when the radius of curvature began decreasing steadily at 2.2 Myr. The largest decrease in R_c occurred in the early stages of slab sinking as the plate began bending and delaminating from the surface. The R_c in all delamination models increased slightly when the slab tip was deflected by postspinel density inversion at 3.8 Myr. A steady-state peel-back delamination stage was defined as the period of time from 4.0-5.9 Myr with a steadily or weakly decreasing R_c after the slab encountered the 710 km density inversions. The radius of curvature was calculated until the slab began necking prior to slab break-off at 6.5 Myr.

All models with the densest crust (B_{crust} = -175 kg/m^3) delaminated. In order to analyze the effects of variable lithosphere thickness and maximum viscosity, R_c curves were plotted against each other (Fig. 8). Within this subset of models, all R_c evolutions contained the same major characteristic changes as model 5 described in Figure 7. The bending radius during steady-state peel-back delamination was largest for the thickest lithosphere (h_L = 300 km) and decreased with decreasing plate thickness. Delamination occurred on shorter timescales for the thickest plates and initiation timescales increased with decreasing plate thickness. When lithosphere thickness was the same, the weaker plates (i.e. those with lower maximum viscosity) underwent delamination on shorter timescales than stronger plates with higher maximum viscosity.

3.2.2 Topography

Surface topography was calculated every 50 time steps for all delamination models. As the plate began to delaminate, a topographic low developed at the trench near the delamination hinge, and a topographic high was associated with the flexural bulge behind the trench of the bending plate. The height and location of the forebulge and the depth and location of the trench were tracked over time and used to estimate the timing of the end of steady-state peel-back delamination. Specific changes in trench depth, forebulge height, and their locations were identified as a precursor to slab break-off (Supplementary Fig. 1). Viscous necking at the plate hinge during slab break-off indicated the end of steady-state delamination.

3.2.3 Delamination Timescale Analysis

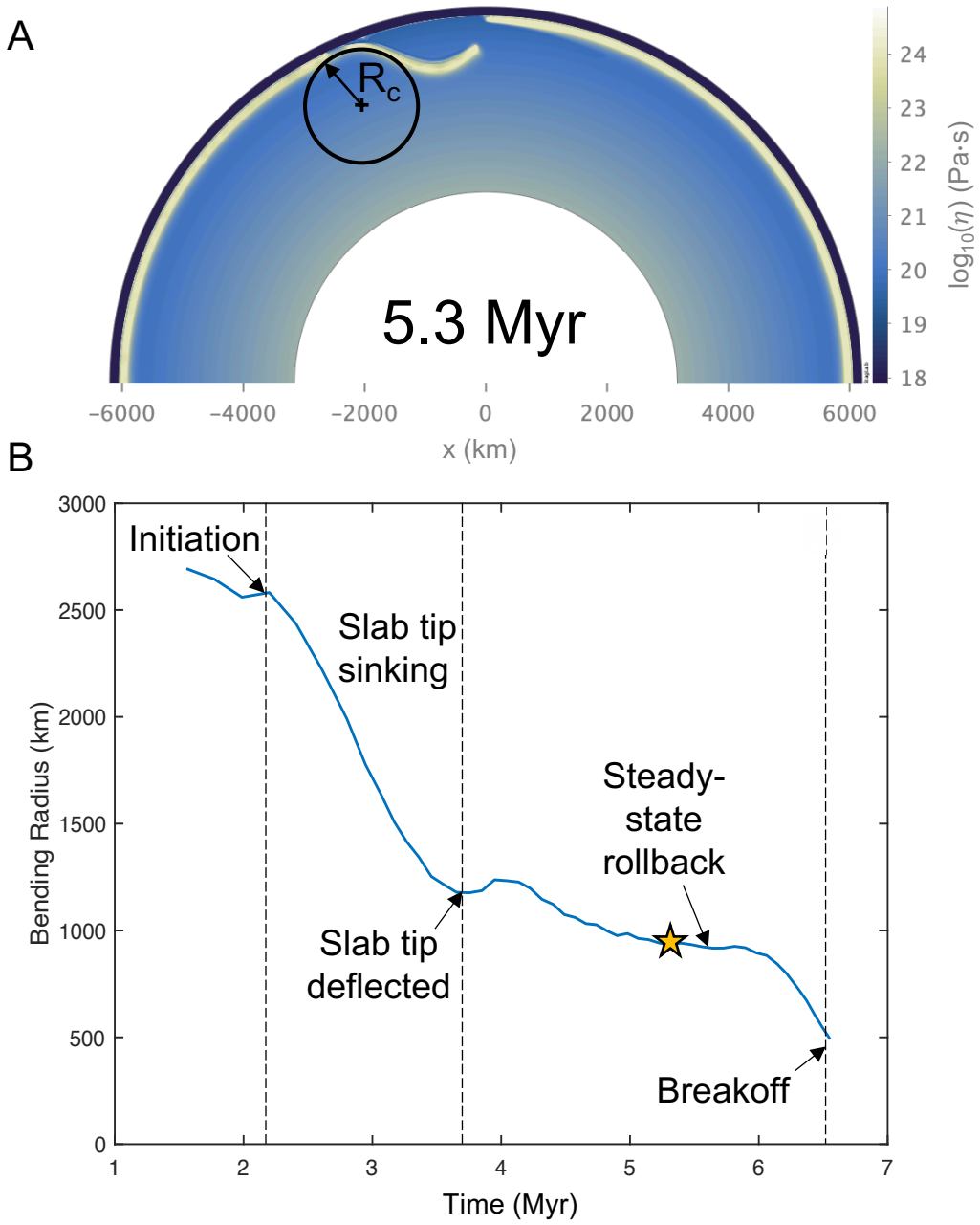

Figure 7. A least squares approximation of a circle to the 1100 K isotherm was used to estimate the radius of curvature, (R_c), during delamination. (A) The R_c for model 5 with B_{crust} = -175 kg/m^3, 250 km-thick lithosphere, and $\eta_{max} = 10^{24}$ Pa·s at t = 5.3 Myr is 930.74 km (indicated by star symbol). (B) The evolution of the R_c over time for the same model. All delamination models exhibit the following features in their respective R_c evolutions: At the onset of delamination, the radius of curvature decreases sharply as the slab tip begins bending and sinking. The R_c increases briefly as the slab encounters the postspinel phase transition and then decreases slightly until reaching a relatively constant value throughout a period of steady-state peel-back delamination. The R_c decreases sharply during slab break-off.

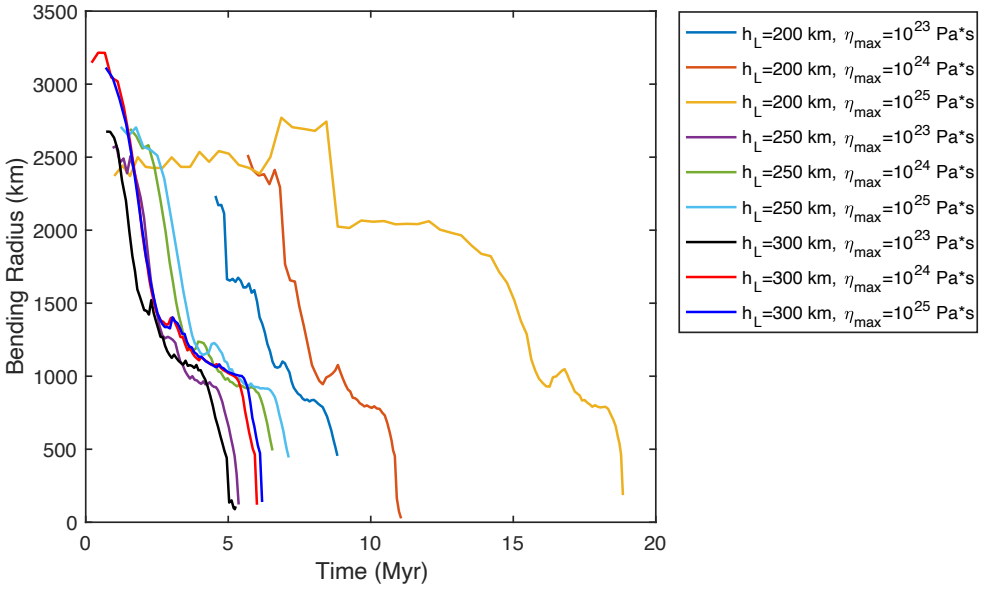

Figure 8. Radius of curvature evolution for all models with B_{crust} = -175 kg/m^3, which represents the least buoyant crust. This subset of models was selected because all cases resulted in delamination and no models were excluded due to being stagnant-lid. All models began at time t=0, but the R_c data begin when initial plate bending was detected and end prior slab break-off. Delamination occurs on faster timescales with increasing plate thickness and decreasing maximum viscosity. Maximum viscosity plays a larger role in delamination timescales when the plate is thinner and closer to neutral buoyancy.

The timescales of delamination initiation and completion were determined using the radius of curvature and topography analyses, respectively, and plotted for each delamination model (Fig. 9). Increasing plate thickness, h_L, generally decreased the timescales for a delamination event to occur. Weaker plates with a lower maximum viscosity delaminated on faster timescales than plates with a higher maximum viscosity. The effect of maximum viscosity became increasingly significant for increasing positive plate buoyancy (decreasing h_L and/or decreasing B_{crust}). The duration of delamination events also increased with increasing maximum plate viscosity. For example, a full delamination event took 1.34 Myr in model 40 ($\eta_{max} = 10^{23}$ Pa·s), took 3.93 Myr in model 41 ($\eta_{max} = 10^{24}$ Pa·s), and took 6.77 Myr in model 42 ($\eta_{max} = 10^{25}$ Pa·s). This effect became stronger with increasing crustal buoyancy (decreasing B_{crust}).

3.2.4 Net Plate Buoyancy

On Earth, subduction is driven by the negative buoyancy of oceanic plates with respect to the underlying mantle. The net buoyancy of the lithosphere can be used to determine if a plate has a propensity to sink or remain at the surface. Net plate buoyancy was controlled by two of the three variables in our parameter space: lithosphere thickness and crust density. Increasing both crust density and lithosphere thickness increases the net negative buoyancy of the plate. The total density of each plate was calculated as a function of depth, including both thermal and compositional components (Fig. 10). A density profile was calculated for each combination of lithosphere thickness and crustal buoyancy in the model suite. The density profiles were integrated over depth to obtain a single value, $\Delta\rho_{plate}$, describing the net density contrast of the plate with respect to the underlying mantle:

$$\Delta\rho_{plate} = \int_0^{h_L} (\rho(z) - \rho_0)\, dz \tag{5}$$

The outcomes of all models are plotted in a regime diagram as a function of the net plate buoyancy and maximum viscosity (Fig. 11). All plates that were negatively buoyant with respect to the underlying mantle delaminated; however, a subset of positively buoyant plates delaminated as well. This highlights a key difference between the mechanisms driving subduction and delamination: negative net plate buoyancy is not required for lithospheric recycling via peel-back delamination.

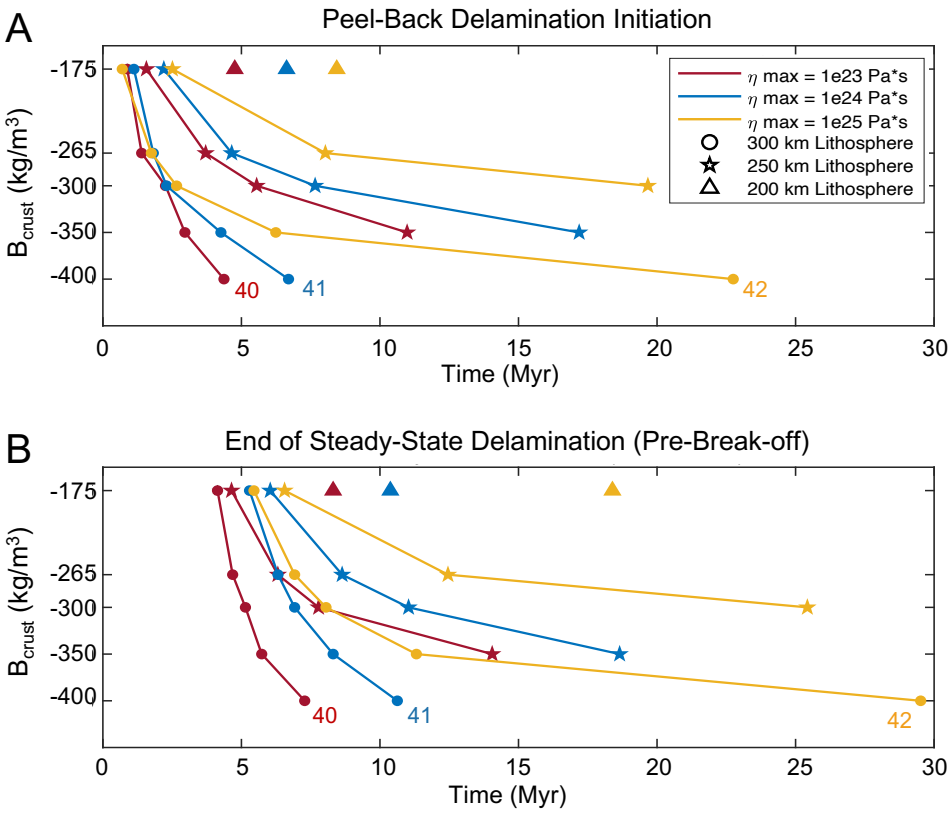

Figure 9. The timing of delamination initiation (top) and the end of steady-state delamination (bottom) are plotted for each model that underwent peel-back delamination. Solid lines connect models with identical maximum viscosity and lithosphere thickness to highlight the effect of varying crustal buoyancy. Model numbers (see Table 2) are included for models that are discussed in this section.

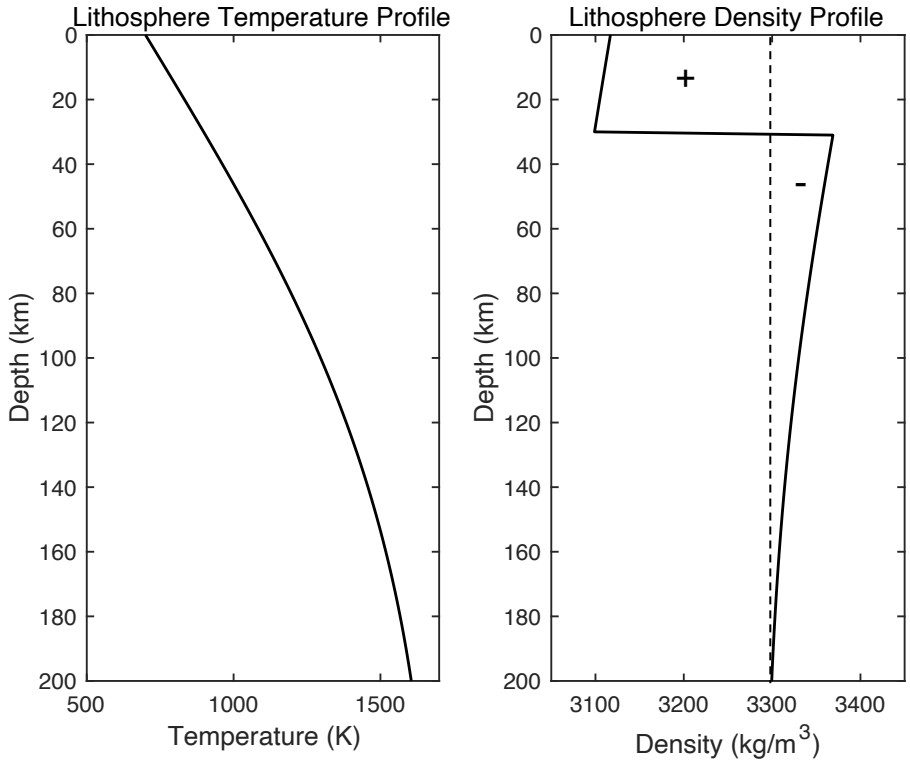

Figure 10. The temperature profile through the depth of the lithosphere (left) is used to calculate the density profile through depth (right) for each combination of lithosphere thickness and crustal buoyancy. Shown here is a 200 km-thick plate with B_{crust} = -265 kg/m^3 corresponding to models 10-12. The density profile includes both compositional and thermal density contributions. The reference density of the underlying mantle, ρ_0 = 3300 kg/m^3, (dotted line) differentiates positively and negatively buoyant regions within the lithosphere.

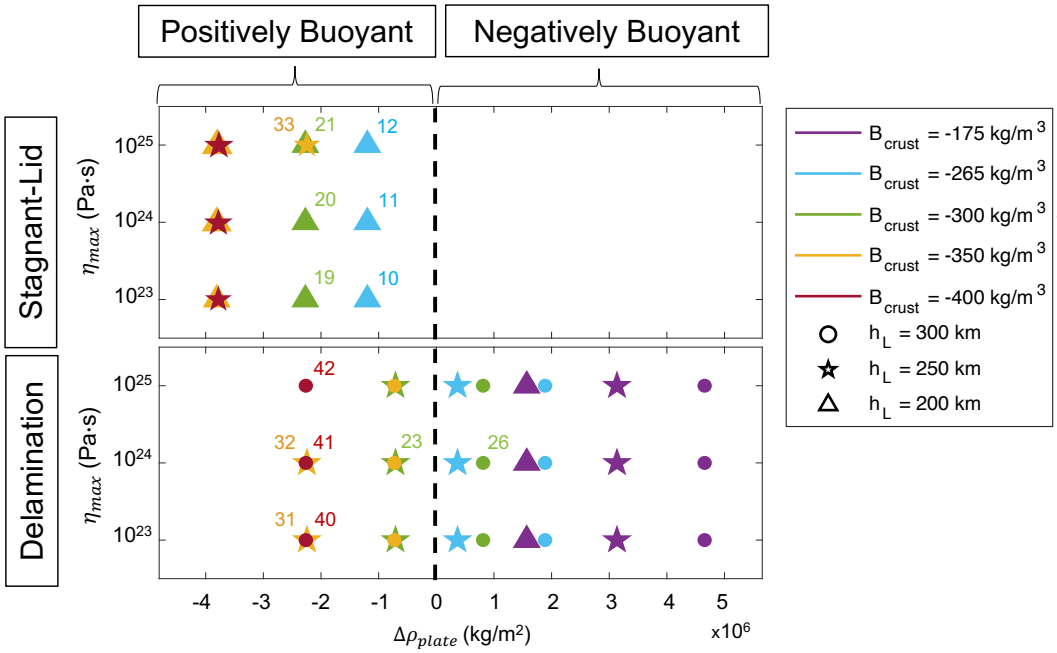

Figure 11. Tectonic regime outcomes are plotted for maximum viscosity vs integrated plate density. Stagnant-lid models (top) are separated from delamination models (bottom). Model numbers (see Table 2) are included for those mentioned in the discussion. Plates with a positive integrated density contrast ($\Delta\rho_{plate}$) with respect to the underlying mantle have a net negative plate buoyancy, while a negative $\Delta\rho_{plate}$ corresponds to a net positive plate buoyancy. All negatively buoyant plates delaminated. A subset of positively buoyant plates also delaminated (lower left quadrant), even though other models with nearly identical net plate buoyancy were stagnant-lid.

4 Discussion

4.1 Peel-Back Delamination Initiation

To understand why certain positively buoyant plates delaminate but others with the same net buoyancy do not, we must understand the mechanisms driving peel-back delamination. Delamination is a form of lithospheric recycling in which the sub-crustal lithospheric mantle (SCLM) detaches and peels away from a layer of overlying crust remaining at the surface. Peel-back delamination propagates along the Moho (the largest strength discontinuity over the depth of the plate) where weak, buoyant crust is juxtaposed with stronger, more negatively buoyant lithospheric mantle. Like subduction, the delamination mechanism is primarily driven by the excess density of the lithospheric mantle with respect to the underlying asthenosphere (Bird, 1979). Thus, delamination is facilitated by plates having a thick, negatively buoyant mantle lithosphere.

We model a compositionally-homogeneous upper mantle, so the colder lithospheric mantle is always negatively buoyant with respect to the sub-lithospheric mantle. However, delamination is resisted by (1) the coupling of the plate across the lower crust-upper mantle boundary and (2) the viscous strength of the mantle. A low-viscosity lower crust layer allows mechanical decoupling along the crust-mantle boundary which is crucial for delamination to occur (Chen, 2021; Göğüş & Ueda, 2018; Krystopowicz & Currie, 2013; Magni et al., 2013; Meissner & Mooney, 1998). Early in our delamination model evolutions, the yield strength of the crust is exceeded near the plate edge due to vertical tensile stresses resulting from the initial displacement of the gravitationally unstable lithospheric mantle. Consequently, the yielded crust forms a low-viscosity layer which facilitates decoupling of the crust from the lithospheric mantle. The amount of crustal yielding increases by increasing the thickness of the lithosphere and therefore increasing its negative buoyancy (Fig. 12). Within the subset of net positively buoyant plates, the thickest plates (h_L = 300 km) always subducted while the thinnest plates (h_L = 200 km) always remained stagnant-lid. This dichotomy was observed when the 200 and 300 km-thick plates had nearly identical net plate buoyancy (Fig. 11: see models 19-21 vs models 38-40). Even when the 200 km plate was more net negatively buoyant than the 300 km plate, it still remained stable in the stagnant lid regime (Fig. 11: see models 10-12

vs models 38-40). The thinner lithosphere to the right of the gap (h_{L-min} = 100 km) never delaminated because there is less negative buoyancy to overcome the coupling of the crust and lithosphere. When the lithospheric mantle portion of the plate is sufficiently dense, the forces driving delamination prevail; however when the lithospheric mantle has insufficient negative buoyancy, plate coupling inhibits delamination.

It is worth reiterating that delamination is driven by the negative buoyancy of the lithospheric mantle with respect to the underlying mantle, and not the density contrast across the Moho. While it may be seem reasonable to assume that increasing the density contrast between the crust and lithosphere would always promote decoupling, varying crustal buoyancy has a more complicated effect. This can be observed in the subset of positively buoyant plates with a 250 km-thick lithosphere: those closer to neutral buoyancy delaminated (B_{crust} = [-300, -350] kg/m^3), while increasing crustal buoyancy favored a stagnant-lid outcome (B_{crust} = [-350, -400] kg/m^3) (Fig. 11). Although the lithospheric mantle portion of the plate maintained the same integrated negative buoyancy, increasing the positive buoyancy of the crust (and therefore the entire plate) inhibits delamination. The positive buoyancy of the crust resists plate bending, thereby preventing crustal yielding and the development of the weak zone required for delamination. Compared to thicker plates with excess negative buoyancy, thinner plates require less positively buoyant crust in order to undergo bending and delamination.

4.2 Plate Strength

In addition to plate coupling across the crust-mantle boundary, the viscous strength of the mantle is another resisting force to delamination. By varying the maximum viscosity of our models over two orders of magnitude [10^{23}, 10^{24}, 10^{25} Pa·s], we systematically varied the strength of the cold upper portion of the lithosphere. The energy required for plate bending is proportional to its viscosity; therefore plate bending, which is required for the formation of the delamination weak zone, becomes more difficult with increasing maximum viscosity. For example, models 32 and 33 were identical except for a one order-of-magnitude difference in maximum viscosity ($\eta_{max,32}$ = 10^{24} Pa·s and $\eta_{max,33}$ = 10^{25} Pa·s). The weaker plate in model 32 delaminated while the stronger plate in model 33 remained a stagnant lid (Fig. 13). The effect of increasing maximum viscosity can further be observed in the timescales of delamination (Fig. 9). In models with otherwise identical parameters, increasing maximum viscosity increases the timescales of the de-

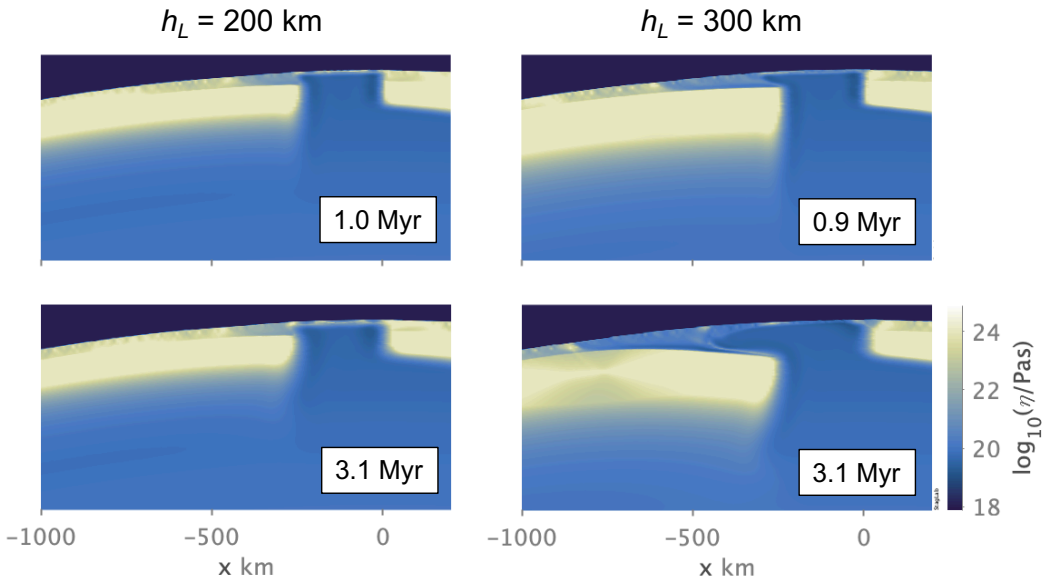

Figure 12. Viscosity field comparison of crust yielding and weak zone formation for stagnant-lid model 20 (left) vs. delamination model 26 (right). Models were identical (B_{crust} = -300 kg/m^3, $\eta_{max} = 10^{24}$ Pa·s) except for plate thickness. The 300 km-thick plate in model 26 has a thicker and denser lithospheric mantle, causing it to bend further and induce more crustal yielding over the plate edge. The yielded crust is weak and facilitates decoupling and delamination of the lithospheric mantle. Although some crust weakening is observed over the plate edge of model 20, its thinner lithospheric mantle has less negative buoyancy to form a sufficient delamination weak zone. If the crust is yielded but delamination is not initiated (left), the strength (i.e. viscosity) of the weakened crust increases over time.

lamination process because it takes longer to bend stronger plates. The effect of maximum viscosity on delamination timing becomes increasingly important at higher values of crustal buoyancy. When the crust is more positively buoyant, it takes significantly longer for the strongest plates to go unstable than the equivalent models with lower maximum viscosity.

The viscous strength of the mantle as a resisting force to delamination not only refers to the strength of the plate itself, but also the resistance of the sublithospheric mantle to deformation from a sinking plate. Although we did not vary the radial viscosity over the depth of the mantle, a higher viscosity asthenosphere would inhibit delamination and prolong timescales of delamination, while a weak asthenosphere may promote delami-

nation on shorter timescales. We used a single value for mantle potential temperature (1700 K), but we expect that higher temperatures would favor delamination on shorter timescales. A warmer interior would decrease the viscosity of the sublithospheric mantle, which would facilitate delamination. Warmer mantle temperatures and higher temperature gradients across the lithosphere would reduce plate strength, which would also facilitate plate bending and delamination. Conversely, a colder mantle temperature would likely inhibit delamination and slab sinking. Such details can be pursued by future investigations.

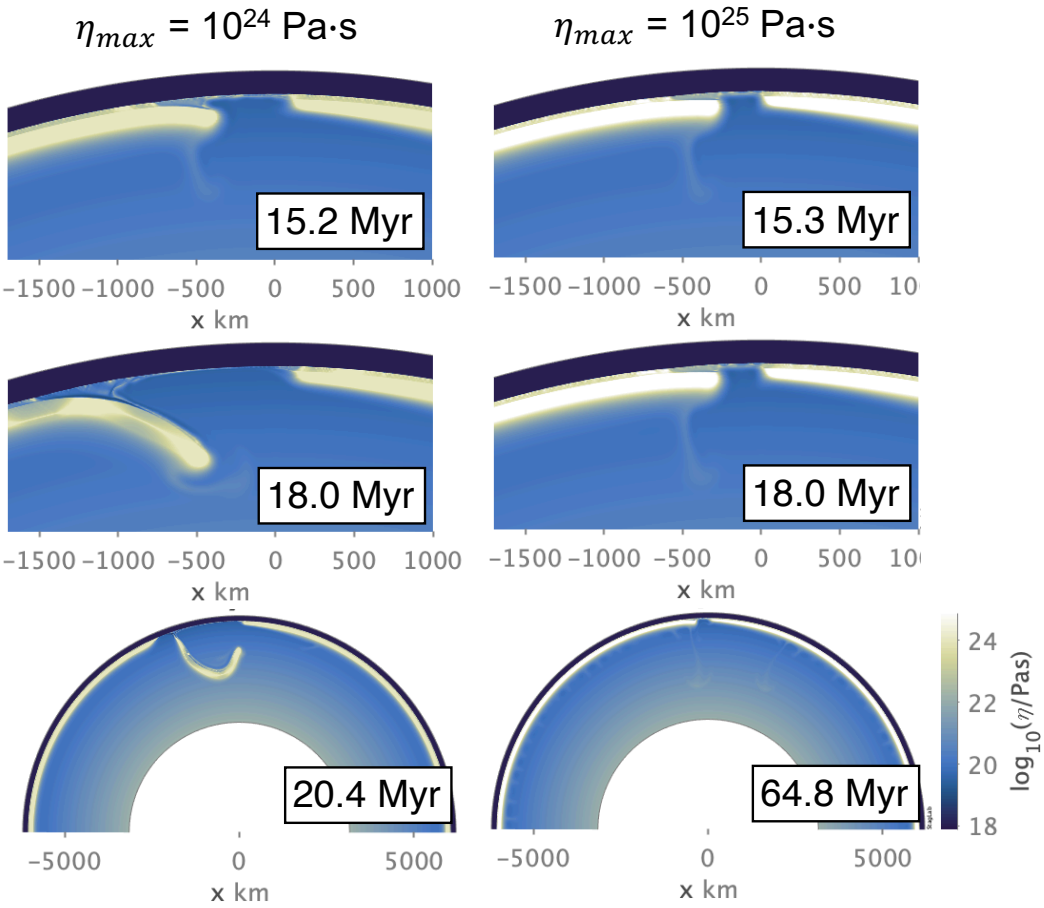

Figure 13. Viscosity field comparison of model 31 with a maximum viscosity of 10^{24} Pa·s (left) vs. model 32 with a maximum viscosity of 10^{25} Pa·s (right). Both plates are positively buoyant with identical net buoyancy, plate thickness (h_L = 250 km) and crust buoyancy (B_{crust} = -350 kg/m^3). The weaker plate is able to undergo bending and delamination, yet only a one order-of-magnitude increase in viscosity causes the stronger plate to resist bending and remain immobile.

4.3 Crustal Thickness and Buoyancy

Gravity and topography predict large regional variations in Venus' crustal thickness (0-110 km) (Anderson & Smrekar, 2006) and estimates for the average crustal thickness typically fall between 8-50 km (James et al., 2013). Variations in crustal thickness may have a complicated effect on delamination initiation. On one hand, thicker layers of buoyant crust will increase the positive buoyancy of the plate and inhibit plate bending and delamination. However, increasing crustal thickness in our models would result in less cold, strong lithospheric mantle to resist plate bending. The basalt-eclogite transition occurs at deeper depths in Venus' mantle than on Earth, requiring crust to subduct to deeper depths before the added negative buoyancy from eclogite can help sustain delamination. Yet if crust on Venus is thicker than on Earth, less crust displacement is necessary for eclogitization depths to be reached. If we consider a multi-stage basalt-eclogite transition beginning at shallower depths than 70 km (Ito & Kennedy, 1971), a thick layer of crust may reduce the compositional buoyancy of the crust and stimulate recycling of the lower crust and lithosphere on faster timescales.

Not all models of global episodic overturns consider the chemical buoyancy of the crust and its effect on subduction (Weller & Kiefer, 2020), and others may underestimate its effect (Armann & Tackley, 2012; Crameri & Tackley, 2016; Rolf et al., 2018; Uppalapati et al., 2020). To isolate the effect of crustal buoyancy on lithospheric recycling, we varied the density contrast of the crust, B_{crust}, over 5 values (-175 to -400 kg/m^3) for a uniformly-thick crust (h_{crust} = 30 km). Our results indicate that the chemical buoyancy of the crust is an important factor understanding delamination initiation because it (1) affects the net buoyancy of the plate and (2) resists the bending of the lithospheric mantle that is a precursor to delamination. More work will need to be done to understand the role that crustal thickness and buoyancy play on the different styles of resurfacing proposed for Venus.

4.4 Yield Stress

For Earth, there is a discrepancy between the maximum yield stress predicted by laboratory experiments (Kohlstedt et al., 1995) and those used in numerical models to study subduction (Tackley, 2008). A mobile-lid is generally favored when the yield stress parameterization is limited by a low maximum yield stress with depth, and increasing the maximum yield stress promotes a stagnant-lid (Moresi & Solomatov, 1998). Armann

and Tackley (2012) found that 5-8 global overturns can occur when the yield stress is limited to 100 MPa (Armann & Tackley, 2012) and other studies have modeled global overturns on Venus by employing similarly low yield stresses (Crameri & Tackley, 2016; Rolf et al., 2018; Weller & Kiefer, 2020; Uppalapati et al., 2020). Higher yield stresses (up to 300 MPa) also produced global overturns, though the duration of the mobile-lid period was shorter and less vigorous (Armann & Tackley, 2012).

Since the yield strength profile with depth is even less constrained for Venus, we tested a higher limiting yield stress (500 MPa) than in previous global overturn models. We were able to model regional-scale lithospheric resurfacing with a relatively high yield stress in part because the the crust strength is limited by a relatively low yield stress (surface cohesion = 10 MPa). Venus' lower crust is predicted by some to be weak relative to the upper crust and underlying lithospheric mantle and deformable on relatively short geologic timescales (Arkani-Hamed, 1993; Azuma et al., 2014; Buck, 1992; Ghail, 2015; Katayama, 2021; Zuber, 1987). Previous experimental studies may have overestimated the strength of Venus' crust (Mackwell et al., 1998) by using diabase instead of plagioclase at the brittle-ductile transition where Peierls creep is the primary deformation mechanism (Azuma et al., 2014; Katayama, 2021). We also consider that crustal yielding and weak zone formation is driven by tensile forces in the crust owing to the gravitational instability of the lithospheric mantle. In this context, a weak crust parameterization may be appropriate since the yield strength of the crust is expected to be lower in tension than compression. A higher crustal yield strength would inhibit weak zone formation; delamination would likely require thicker lithospheres in order to generate sufficient stresses in the crust.

Still, the weak zone could come from a variety of tectonic processes, including melting and intrusive magmatism in the lithosphere (Lourenço et al., 2020). If there was a pre-existing weak zone in the plate that did not require crustal yielding, it is possible that thinner plates may also undergo delamination. Higher strength crust may still yield and form a weak zone in the presence higher lithospheric stresses due to ongoing tectonic deformation. The origin of the weak zone is not considered to be within the scope of this study but is important in understanding how delamination could operate on Venus.

4.5 Uncertainties

In our simplified rift zone setup, we model a sharp temperature gradient across a vertical boundary separating the plate edge and the gap containing relatively warm mantle material. The lithospheric gap itself is only a first order representation for the thermal structure at rift zones on Venus and lacks finer details. However, it is an appropriate starting point as we acquire a better understanding of the relationship between the strength and buoyancy of a plate and its tendency to delaminate.

In the early stages of delamination, only a thin layer of crust is attached to the downgoing plate. Once the crustal root reaches the eclogite transition depth, thicker layers of crust remain attached to the delaminating plate due to the eclogite density inversion (see Fig. 6). The thickness of the crustal root over the delamination hinge is important in determining how much crust is eclogitzed, which has implications for slab sinking dynamics. We imposed a minimum crust thickness of 15 km to prevent sticky-air particles from becoming embedded in the mantle material exposed at the surface of the gap due to its low viscosity contrast. Though this feature may potentially overestimate the amount of crust at the surface, we expect that new crust would be generated in the delamination zone. Since our models currently do not include melting processes, the volume of crust at the surface is an approximation.

4.5 Implications for Resurfacing

A peel-back delamination event on Venus would undoubtedly have a unique surface expression. During the initial stages of delamination, it is clear that the majority of the crust remains at the surface or within the crustal root formed at the slab hinge (Fig. 4D). As the lithospheric mantle peels away, it is replaced by warm asthenosphere flowing beneath a thinned layer of crust at the surface. Delamination of the lithospheric mantle in Earth-like conditions is predicted to lead to enhanced surface magmatism, local tectonic uplift, and horizontal surface deformation in the region overlying the delamination zone (Bird, 1979; Göğüş & Pysklywec, 2008; Kay & Kay, 1993). Yet, due to uncertainties in the exact volume of remaining surface crust, the style and extent of resurfacing that may follow a delamination event still remains unclear. Perhaps the delamination zone would be fully resurfaced due to a high degree of induced surface volcanism - or perhaps delamination may only be a source of surface deformation and crater modification via localized, thin lava flows consistent with the regional equilibrium resurfacing model (O'Rourke et al., 2014).

Without modeling melt processes, the extent of resurfacing will remain unclear. However, we can compare our results to delamination models in an Archean Earth environment (Chowdhury et al., 2017, 2020; Perchuk et al., 2018) when the mantle was thought to be hotter and more comparable to Venus than at present (Herzberg et al., 2010). Our initial condition resembles the starting point for the initiation of "peel back convergence" in a numerical modeling study of delamination in the Archean Earth by Chowdhury et al. (2020) (see their Fig. 1c). Peel back convergence is described as a form of rollback delamination initiated at a sharp lateral lithospheric discontinuity at a convergent margin (Chowdhury et al., 2020). While the weak zone delamination surface in our models originated from yielding of a weak lower crust, the weak zone in Chowdhury et al. (2020) was generated by melting and weakening of a protocontinental crust. Following a delamination event, they observed a region of thinned, hot crust at the surface characterized by localized volcanism, including underplating melt and rising melt domes. For a more modern analogue, the Cenozoic evolution of the Hellenides retreating subduction system may be appropriate. The Hellenides are associated with extension in the overriding plate and regional compression at the overriding plate edge (Brun et al., 2016; Burchfiel et al., 2018; Vassilakis et al., 2011). The hot, thinned crust over the delamination zone may undergo a similar mode of back-arc extension shown to accompany trench retreat and slab rollback.

In addition to the surface expression of a delamination event, is also important to constrain the total delamination area in order to understand the extent of resurfacing that is possible. We estimate the total length of a single peel-back delamination event to be between 2500-3000 km (approximately 1/7 of the surface). Since our models are two dimensional, we possibly over- or underestimate the scale of the delamination zone. Future directions may include modeling peel-back delamination in 3D, since three-dimensional models are important for understanding the mantle dynamics and tectonics associated with the toroidal component of flow induced by a sinking slab (Stegman et al., 2006; Schellart et al., 2007). This may have implications for slab sinking geometry, predicted melt volumes, and total amount of resurfacing that may occur during a delamination event.

5 Conclusions

Despite the thousands of kilometers of rift zones that have been identified as potential subduction sites on Venus (Sandwell & Schubert, 1992; Schubert & Sandwell, 1995),

there have been no studies to date which have investigated the dynamics of lithospheric recycling initiated at Venusian rift zones. Here, we presented the first 2D numerical models to indicate that peel-back delamination initiated at a lateral lithospheric discontinuity may be a viable mechanism for lithospheric recycling and heat loss on Venus. Delamination has been proposed to occur on Venus, however it is typically studied within the context of plume-lithosphere interactions and coronae formation (Ashwal et al., 1988; Davaille et al., 2017; Gülcher et al., 2020; Hoogenboom & Houseman, 2006; Piskorz et al., 2014; Smrekar & Stofan, 1997). We showed that in the absence of plume-lithosphere interactions, the full depth of the sub-crustal lithospheric mantle can detach and peel away from the crust remaining at the surface.

Delamination is primarily driven by the excess density of the lithospheric mantle. It requires a weak lower crust for decoupling to propagate and a connection between the Moho and asthenosphere for buoyant material to rise and fill the space between the crust and down-going plate. When these criteria are satisfied we observe that, unlike subduction, both net positive and net negatively buoyant plates may undergo delamination. Our results indicate that positive crustal buoyancy inhibits delamination by impeding plate bending which drives crust yielding and weak zone formation. However once the crust reaches the basalt-eclogite transition depth, the eclogite density inversion helps sustain delamination. Delamination may only occur when the mantle lithosphere is sufficiently negatively buoyant to bend and counteract the initial positive buoyancy of the crust. In cases with insufficient mantle lithosphere thickness, excess crustal buoyancy, or the absence of a conduit connecting crust and asthenosphere, a stagnant-lid regime may persist.

Peel-back delamination may have important implications as a source of regional-scale resurfacing within the framework of the regional equilibrium resurfacing (RER) hypothesis. Following a delamination event, the emplacement of hot asthenosphere beneath a layer of thinned crust may enhance surface deformation and volcanism. Perhaps the evidence for the highly deformed (Byrne et al., 2020) and globally fragmented lithosphere (Byrne et al., 2021) can be viewed as forms of surface tectonics associated with delamination events. Not only is delamination compatible with Venus' style of surface deformation, but it may be responsible for some of the observed heterogeneity in crust and lithosphere thickness (Borrelli et al., 2021). Though more work will need to be done to determine if it can satisfy cratering and CM-CF offset constraints, the regional-scale peel-

back delamination regime may be able to explain some aspects of Venus' unique resurfacing history.

Acknowledgments

Authors are grateful for support from NASA Award 80NSSC22K0100. Computational resources were provided by Extreme Science and Engineering Discovery Environment (XSEDE), which is supported by National Science Foundation grant number ACI-1053575. The authors would like to thank David Sandwell for helpful discussions. A. Adams also thanks CIG for travel support to 2019 Ada Lovelace Workshop on Modelling Mantle and Lithosphere Dynamics.

6 Open Research

The model data from this study are available in an online repository (Adams, 2022).

References

Adams, A. C. (2022). *Regional-scale lithospheric recycling on venus via peel-back delamination.* Zenodo. Retrieved from `https://doi.org/10.5281/zenodo.6819751` doi: 10.5281/zenodo.6819751

Akaogi, M., & Ito, E. (1993). Refinement of enthalpy measurement of mgsio 3 perovskite and negative pressure-temperature slopes for perovskite-forming reactions. *Geophysical Research Letters*, *20*, 1839-1842. doi: 10.1029/93GL01265

Anderson, F. S., & Smrekar, S. E. (2006). Global mapping of crustal and lithospheric thickness on venus. *Journal of Geophysical Research E: Planets*, *111*. doi: 10.1029/2004JE002395

Arkani-Hamed, J. (1993). On the tectonics of venus. *Physics of the Earth and Planetary Interiors*, *76*, 75-96. doi: 10.1016/0031-9201(93)90056-F

Armann, M., & Tackley, P. J. (2012). Simulating the thermochemical magmatic and tectonic evolution of venus's mantle and lithosphere: Two-dimensional models. *Journal of Geophysical Research: Planets*, *117*. doi: 10.1029/2012JE004231

Ashwal, L. D., Burke, K., & Sharpton, V. L. (1988). Lithospheric delamination on earth and venus. *Abstracts of the Lunar and Planetary Science Conference*, *19*, 17.

Azuma, S., Katayama, I., & Nakakuki, T. (2014). Rheological decoupling at the

moho and implication to venusian tectonics. *Scientific Reports*, *4*, 1-5. doi: 10.1038/srep04403

Basilevsky, A. T., & Head, J. W. (2002). Venus: Timing and rates of geologic activity. *Geology*, *30*, 1015. doi: 10.1130/0091-7613(2002)030⟨1015:VTAROG⟩2.0.CO;2

Bird, P. (1979). Continental delamination and the colorado plateau. *Journal of Geophysical Research*, *84*. doi: 10.1029/JB084iB13p07561

Bjonnes, E. E., Hansen, V. L., James, B., & Swenson, J. B. (2012). Equilibrium resurfacing of venus: Results from new monte carlo modeling and implications for venus surface histories. *Icarus*, *217*, 451-461. doi: 10.1016/j.icarus.2011.03.033

Borrelli, M. E., O'Rourke, J. G., Smrekar, S. E., & Ostberg, C. M. (2021). A global survey of lithospheric flexure at steep-sided domical volcanoes on venus reveals intermediate elastic thicknesses. *Journal of Geophysical Research: Planets*, *126*. doi: 10.1029/2020JE006756

Brun, J. P., Faccenna, C., Gueydan, F., Sokoutis, D., Philippon, M., Kydonakis, K., & Gorini, C. (2016). The two-stage aegean extension, from localized to distributed, a result of slab rollback acceleration. *Canadian Journal of Earth Sciences*, *53*, 1142-1157. doi: 10.1139/cjes-2015-0203

Buck, W. R. (1992). Global decoupling of crust and mantle: Implicatons for topography, geoid and mantle viscosity on venus. *Geophysical Research Letters*, *9*, 2111-2114. doi: 10.1029/92GL02462

Bullock, M. A., Grinspoon, D. H., & Head, J. W. (1993). Venus resurfacing rates: Constraints provided by 3-d monte carlo simulations. *Geophysical Research Letters*, *20*, 2147-2150. doi: 10.1029/93GL02505

Burchfiel, B. C., Royden, L. H., Papanikolaou, D., & Pearce, F. D. (2018). Crustal development within a retreating subduction system: The hellenides. *Geosphere*, *14*, 1119-1130. doi: 10.1130/GES01573.1

Byrne, P. K., Ghail, R. C., Gilmore, M. S., Şengör, A. M., Klimczak, C., Senske, D. A., ... Solomon, S. C. (2020, 1). Venus tesserae feature layered, folded, and eroded rocks. *Geology*, *49*, 81-85. doi: 10.1130/G47940.1

Byrne, P. K., Ghail, R. C., Şengör, A. M., James, P. B., Klimczak, C., & Solomon, S. C. (2021). A globally fragmented and mobile lithosphere

on venus. *Proceedings of the National Academy of Sciences*, *118*. doi: 10.1073/pnas.2025919118

Chen, L. (2021). The role of lower crustal rheology in lithospheric delamination during orogeny. *Frontiers in Earth Science*, *9*. doi: 10.3389/feart.2021.755519

Chowdhury, P., Chakraborty, S., Gerya, T. V., Cawood, P. A., & Capitanio, F. A. (2020). Peel-back controlled lithospheric convergence explains the secular transitions in archean metamorphism and magmatism. *Earth and Planetary Science Letters*, *538*. doi: 10.1016/j.epsl.2020.116224

Chowdhury, P., Gerya, T., & Chakraborty, S. (2017). Emergence of silicic continents as the lower crust peels off on a hot plate-tectonic earth. *Nature Geoscience*, *10*, 698-703. doi: 10.1038/ngeo3010

Crameri, F. (2018). Geodynamic diagnostics, scientific visualisation and staglab 3.0. *Geoscientific Model Development*, *11*, 2541-2562. doi: 10.5194/gmd-11-2541-2018

Crameri, F., Schmeling, H., Golabek, G. J., Duretz, T., Orendt, R., Buiter, S. J. H., ... Tackley, P. J. (2012). A comparison of numerical surface topography calculations in geodynamic modelling: an evaluation of the 'sticky air' method. *Geophysical Journal International*, *189*, 38-54. doi: 10.1111/j.1365-246X.2012.05388.x

Crameri, F., & Tackley, P. J. (2016). Subduction initiation from a stagnant lid and global overturn: new insights from numerical models with a free surface. *Progress in Earth and Planetary Science*, *3*. doi: 10.1186/s40645-016-0103-8

Davaille, A., Smrekar, S. E., & Tomlinson, S. (2017). Experimental and observational evidence for plume-induced subduction on venus. *Nature Geoscience*, *10*, 349-355. doi: 10.1038/ngeo2928

Davies, G. F. (2008). Episodic layering of the early mantle by the 'basalt barrier' mechanism. *Earth and Planetary Science Letters*, *275*, 382-392. doi: 10.1016/j.epsl.2008.08.036

Fei, Y., Orman, J. V., Li, J., van Westrenen, W., Sanloup, C., Minarik, W., ... Funakoshi, K. (2004). Experimentally determined postspinel transformation boundary in mg2sio4 using mgo as an internal pressure standard and its geophysical implications. *Journal of Geophysical Research: Solid Earth*, *109*. doi: 10.1029/2003jb002562

Feuvre, M. L., & Wieczorek, M. A. (2011). Nonuniform cratering of the moon and a revised crater chronology of the inner solar system. *Icarus*, *214*, 1-20. doi: 10.1016/j.icarus.2011.03.010

Fukao, Y., Obayashi, M., Nakakuki, T., Utada, H., Suetsugu, D., Irifune, T., ... Hirose, K. (2009). Stagnant slab: A review. *Annual Review of Earth and Planetary Sciences*, *37*, 19-46. doi: 10.1146/annurev.earth.36.031207.124224

Ghail, R. (2015). Rheological and petrological implications for a stagnant lid regime on venus. *Planetary and Space Science*, *113-114*, 2-9. doi: 10.1016/j.pss.2015.02.005

Göğüş, O. H., & Ueda, K. (2018). Peeling back the lithosphere: Controlling parameters, surface expressions and the future directions in delamination modeling. *Journal of Geodynamics*, *117*, 21-40. doi: 10.1016/j.jog.2018.03.003

Göğüş, O. H., & Pysklywec, R. N. (2008). Near-surface diagnostics of dripping or delaminating lithosphere. *Journal of Geophysical Research: Solid Earth*, *113*. doi: 10.1029/2007JB005123

Gülcher, A. J., Gerya, T. V., Montési, L. G., & Munch, J. (2020). Corona structures driven by plume–lithosphere interactions and evidence for ongoing plume activity on venus. *Nature Geoscience*, *13*, 547-554. doi: 10.1038/s41561-020-0606-1

Hansen, V. L., & Young, D. A. (2007). Venus's evolution: A synthesis. *Special Paper of the Geological Society of America*, *419*, 255-273. doi: 10.1130/2006.2419(13)

Hernlund, J. W., & Tackley, P. J. (2008). Modeling mantle convection in the spherical annulus. *Physics of the Earth and Planetary Interiors*, *171*, 48-54. doi: 10.1016/j.pepi.2008.07.037

Herrick, R. R. (1994). Resurfacing history of venus. *Geology*, *22*, 703-706. doi: 10.1130/0091-7613(1994)022⟨0703:RHOV⟩2.3.CO;2

Herrick, R. R., & Rumpf, M. E. (2011). Postimpact modification by volcanic or tectonic processes as the rule, not the exception, for venusian craters. *Journal of Geophysical Research E: Planets*, *116*. doi: 10.1029/2010JE003722

Herzberg, C., Condie, K., & Korenaga, J. (2010). Thermal history of the earth and its petrological expression. *Earth and Planetary Science Letters*, *292*, 79-88. doi: 10.1016/j.epsl.2010.01.022

Hoogenboom, T., & Houseman, G. A. (2006). Rayleigh-taylor instability as a mechanism for corona formation on venus. *Icarus*, *180*, 292-307. doi: 10.1016/j.icarus.2005.11.001

Houseman, G. A., & Molnar, P. (1997). Gravitational (rayleigh-taylor) instability of a layer with non-linear viscosity and convective thinning of continental lithosphere. *Geophysical Journal International*, *128*, 125-150. doi: 10.1111/j.1365-246X.1997.tb04075.x

Irifune, T., Nishiyama, N., Kuroda, K., Inoue, T., Isshiki, M., Utsumi, W., ... Ohtaka, O. (1998). The postspinel phase boundary in mg2sio4 determined by in situ x-ray diffraction. *Science*, *279*, 1698-1700. doi: 10.1126/science.279.5357.1698

Ito, K., & Kennedy, G. C. (1971). An experimental study of the basalt-garnet granulite-eclogite transition. *Geophysical Monography Series*, *14*, 303-314. doi: 10.1029/GM014p0303

Izenberg, N. R., Arvidson, R. E., & Phillips, R. J. (1994). Impact crater degradation on venusian plains. *Geophysical Research Letters*, *21*, 289-292. doi: 10.1029/94GL00080

James, P. B., Zuber, M. T., & Phillips, R. J. (2013). Crustal thickness and support of topography on venus. *Journal of Geophysical Research E: Planets*, *118*, 859-875. doi: 10.1029/2012JE004237

Johnson, T. E., Brown, M., Kaus, B. J., & Vantongeren, J. A. (2014). Delamination and recycling of archaean crust caused by gravitational instabilities. *Nature Geoscience*, *7*, 47-52. doi: 10.1038/ngeo2019

Katayama, I. (2021). Strength models of the terrestrial planets and implications for their lithospheric structure and evolution. *Progress in Earth and Planetary Science*, *8*. doi: 10.1186/s40645-020-00388-2

Katsura, T., Yamada, H., Shinmei, T., Kubo, A., Ono, S., Kanzaki, M., ... Utsumi, W. (2003). Post-spinel transition in mg2sio4 determined by high p-t in situ x-ray diffractometry. *Physics of the Earth and Planetary Interiors*, *136*, 11-24. doi: 10.1016/S0031-9201(03)00019-0

Kay, R. W., & Kay, S. M. (1993). Delamination and delamination magmatism. *Tectonophysics*, *219*, 177-189. doi: 10.1016/0040-1951(93)90295-U

King, S. (2018). Venus resurfacing constrained by geoid and topography. *Journal of*

Geophysical Research: Planets, *123*, 1041-1060. doi: 10.1002/2017JE005475

Kohlstedt, D. L., Evans, B., & Mackwell, S. J. (1995). Strength of the lithosphere: constraints imposed by laboratory experiments. *Journal of Geophysical Research*, *100*, 17587-17602. doi: 10.1029/95JB01460

Krystopowicz, N. J., & Currie, C. A. (2013). Crustal eclogitization and lithosphere delamination in orogens. *Earth and Planetary Science Letters*, *361*, 195-207. doi: 10.1016/j.epsl.2012.09.056

Lourenço, D. L., Rozel, A. B., Ballmer, M. D., & Tackley, P. J. (2020). Plutonic-squishy lid: A new global tectonic regime generated by intrusive magmatism on earth-like planets. *Geochemistry, Geophysics, Geosystems*, *21*. doi: 10.1029/2019GC008756

Mackwell, S. J., Zimmerman, M. E., & Kohlstedt, D. L. (1998). High-temperature deformation of dry diabase with application to tectonics on venus. *JOURNAL OF GEOPHYSICAL RESEARCH*, *103*, 975-984. doi: 10.1029/97JB02671

Magni, V., Faccenna, C., Hunen, J. V., & Funiciello, F. (2013). Delamination vs. break-off: The fate of continental collision. *Geophysical Research Letters*, *40*, 285-289. doi: 10.1002/grl.50090

Martin, P., Stofan, E. R., Glaze, L. S., & Smrekar, S. (2007). Coronae of parga chasma, venus. *Journal of Geophysical Research: Planets*, *112*. doi: 10.1029/2006JE002758

McKinnon, W. B., Zahnle, K. J., Ivanov, B. A., & Melosh, H. J. (1997). Cratering on venus - models and observations in bougher, s.w., hunten, d.m., and phillips, r.j., eds., venus ii geology, geophysics, atmosphere, and solar wind environment. , 969-1014.

Meissner, R., & Mooney, W. (1998). Weakness of the lower continental crust: a condition for delamination, uplift, and escape. *Tectonophysics*, *296*, 47-60. doi: 10.1016/S0040-1951(98)00136-X

Moresi, L., & Solomatov, V. (1998). Mantle convection with a brittle lithosphere: thoughts on the global tectonic styles of the earth and venus. *Geophysical Journal International*, *133*, 669-682. doi: 10.1046/j.1365-246X.1998.00521.x

Namiki, N., & Solomon, S. C. (1994). Impact crater densities on volcanoes and coronae on venus: Implications for volcanic resurfacing. *Science*, *265*, 929-933. doi: 10.1126/science.265.5174.929

Nimmo, F., & McKenzie, D. (1997). Convective thermal evolution of the upper mantles of earth and venus. *Geophysical Research Letters*, *24*, 1539-1542. doi: 10.1029/97GL01382

Ogawa, M., & Yanagisawa, T. (2014). Mantle evolution in venus due to magmatism and phase transitions: From punctuated layered convection to whole-mantle convection. *Journal of Geophysical Research: Planets*, *119*, 867-883. doi: 10.1002/2013JE004593

O'Rourke, J. G., Wolf, A. S., & Ehlmann, B. L. (2014, 12). Venus: Interpreting the spatial distribution of volcanically modified craters. *Geophysical Research Letters*, *41*, 8252-8260. doi: 10.1002/2014GL062121

Parmentier, E. M., & Hess, P. C. (1992). Chemical differentiation of a convecting planetary interior: Consequences for a one plate planet such as venus. *Geophysical Research Letters*, *19*, 2015-2018. doi: 10.1029/92GL01862

Perchuk, A. L., Safonov, O. G., Smit, C. A., van Reenen, D. D., Zakharov, V. S., & Gerya, T. V. (2018). Precambrian ultra-hot orogenic factory: Making and reworking of continental crust. *Tectonophysics*, *746*, 572-586. doi: 10.1016/j.tecto.2016.11.041

Petersen, R. I., Stegman, D. R., & Tackley, P. J. (2017). The subduction dichotomy of strong plates and weak slabs. *Solid Earth*, *8*, 339-350. doi: 10.5194/se-8-339-2017

Phillips, R. J., Arvidson, R. E., Boyce, J. M., Campbell, D. B., Guest, J. E., Schaber, G. G., & Soderblom, L. A. (1991). *Impact craters on venus: Initial analysis from magellan* (Vol. 252). doi: 10.1126/science.252.5003.288

Phillips, R. J., & Hansen, V. L. (1994). Tectonic and magmatic evolution of venus. *Annu. Rev. Earth Planet. Sci.*, *22*, 597-654. doi: 10.1146/annurev.ea.22.050194.003121

Phillips, R. J., & Izenberg, N. R. (1995). Ejecta correlations with spatial crater density and venus resurfacing history. , *22*. doi: 10.1029/95GL01412

Phillips, R. J., Raubertas, R. F., Arvidson, R. E., Sarkar, I. C., Herrick, R. R., Izenberg, N., & Grimm, R. E. (1992). Impact craters and venus resurfacing history. *Journal of Geophysical Research*, *97*, 923-938. doi: 10.1029/92JE01696

Piskorz, D., Elkins-Tanton, L. T., & Smrekar, S. E. (2014). Coronae formation on venus via extension and lithospheric instability. *Journal of Geophysical Re-*

search: Planets, *119*, 2568-2582. doi: 10.1002/2014JE004636

Reese, C. C., Solomatov, V. S., & Moresi, L. N. (1999). Non-newtonian stagnant lid convection and magmatic resurfacing on venus. *Icarus*, *139*, 67-80. doi: 10.1006/icar.1999.6088

Riedel, C., Michael, G. G., Orgel, C., Baum, C., van der Bogert, C. H., & Hiesinger, H. (2021). Studying the global spatial randomness of impact craters on mercury, venus, and the moon with geodesic neighborhood relationships. *Journal of Geophysical Research: Planets*, *126*. doi: 10.1029/2020JE006693

Rolf, T., Steinberger, B., Sruthi, U., & Werner, S. C. (2018). Inferences on the mantle viscosity structure and the post-overturn evolutionary state of venus. *Icarus*, *313*, 107-123. doi: 10.1016/j.icarus.2018.05.014

Sandwell, D. T., & Schubert, G. (1992). Evidence for retrograde lithospheric subduction on venus. *Science*, *257*, 766-770. doi: 10.1126/science.257.5071.766

Schaber, G. G., Strom, R. G., Moore, H. J., Soderblom, L. A., Kirk, R. L., Chadwick, D. J., ... Russell, I. (1992). Geology and distribution of impact craters on venus: What are they telling us? *Journal of Geophysical Research: Planets*, *97*, 257-270. doi: 10.1029/92JE01246

Schellart, W. P. (2010). Evolution of subduction zone curvature and its dependence on the trench velocity and the slab to upper mantle viscosity ratio. *Journal of Geophysical Research: Solid Earth*, *115*. doi: 10.1029/2009JB006643

Schellart, W. P., Freeman, J., Stegman, D. R., Moresi, L., & May, D. (2007). Evolution and diversity of subduction zones controlled by slab width. *Nature*, *446*, 308-311. doi: 10.1038/nature05615

Schubert, G., & Sandwell, D. (1995). A global survey of possible subduction sites on venus. *Icarus*, *117*, 173-196. doi: 10.1006/icar.1995.1150

Shalygin, E. V., Basilevsky, A. T., Markiewicz, W. J., Titov, D. V., Kreslavsky, M. A., & Roatsch, T. (2012). Search for ongoing volcanic activity on venus: Case study of maat mons, sapas mons and ozza mons volcanoes. *Planetary and Space Science*, *73*, 294-301. doi: 10.1016/j.pss.2012.08.018

Shalygin, E. V., Markiewicz, W. J., Basilevsky, A. T., D.V.Titov, Ignatiev, N. I., & Head, J. W. (2015). Active volcanism on venus in the ganiki chasma rift zone. *Geophysical Research Letters*, *42*, 4762-4769. doi: 10.1002/2015GL064088

Shellnutt, J. G. (2016). Mantle potential temperature estimates of basalt from the

surface of venus. *Icarus*, *277*, 98-102. doi: 10.1016/j.icarus.2016.05.014

Smrekar, S. E., & Stofan, E. R. (1997). Corona formation and heat loss on venus by coupled upwelling and delamination. *Science*, *277*(5330), 1289–1294.

Smrekar, S. E., Stofan, E. R., Mueller, N., Treiman, A., Elkins-Tanton, L., Helbert, J., ... Drossart, P. (2010). Recent hotspot volcanism on venus from virtis emissivity data. *Science*, *328*, 605-608. doi: 10.1126/science.1186785

Solomon, S. C., Smrekar, S. E., Bindschadler, I. L. D., Grimm, R. E., Kaula, W. M., McGill, G. E., ... Stofan, E. R. (1992). Venus tectonics: An overview of magellan observations. *Journal of Geophysical Research*, *97*(E8), 13,199-13,255. doi: 10.1029/92JE01418

Stegman, D. R., Freeman, J., Schellart, W. P., Moresi, L., & May, D. (2006). Influence of trench width on subduction hinge retreat rates in 3-d models of slab rollback. *Geochemistry, Geophysics, Geosystems*, *7*. doi: 10.1029/2005GC001056

Strom, R. G., Schaber, G. G., & Dawson, D. D. (1994). The global resurfacing of venus. *Journal of Geophysical Research*, *99*, 899-909. doi: 10.1029/94JE00388

Tackley, P. J. (2008). Modelling compressible mantle convection with large viscosity contrasts in a three-dimensional spherical shell using the yin-yang grid. *Physics of the Earth and Planetary Interiors*, *171*, 7-18. doi: 10.1016/j.pepi.2008.08.005

Turcotte, D. L. (1993). An episodic hypothesis for venusian tectonics. *Journal of Geophysical Research*, *98*, 61-78. doi: 10.1029/93JE01775

Turcotte, D. L. (1995). How does venus lose heat? *Journal of Geophysical Research*, *100*, 16,931-16,940. doi: 10.1029/95JE01621

Turcotte, D. L., Morein, G., Roberts, D., & Malamud, B. D. (1999). Catastrophic resurfacing and episodic subduction on venus. *Icarus*, *139*, 49-54. doi: 10 .1006/icar.1999.6084

Uppalapati, S., Rolf, T., Crameri, F., & Werner, S. C. (2020). Dynamics of lithospheric overturns and implications for venus's surface. *Journal of Geophysical Research: Planets*, *125*. doi: 10.1029/2019JE006258

Vassilakis, E., Royden, L., & Papanikolaou, D. (2011). Kinematic links between subduction along the hellenic trench and extension in the gulf of corinth, greece: A multidisciplinary analysis. *Earth and Planetary Science Letters*, *303*, 108-

120. doi: 10.1016/j.epsl.2010.12.054

Weller, M. B., & Kiefer, W. S. (2020). The physics of changing tectonic regimes: Implications for the temporal evolution of mantle convection and the thermal history of venus. *Journal of Geophysical Research: Planets*, *125*. doi: 10.1029/2019JE005960

Zuber, M. T. (1987). Constraints on the lithospheric structure of venus from mechanical models and tectonic surface features. *Journal of Geophysical Research*, *92*, E541-E551. doi: 10.1029/JB092iB04p0E541

Supporting Information for "Regional-Scale Lithospheric Recycling on Venus via Peel-Back Delamination"

A. C. Adams[1], D. R. Stegman[1], S. E. Smrekar[2], P. J. Tackley[3]

[1]Institute of Geophysics and Planetary Physics, Scripps Institution of Oceanography, University of California, San Diego, CA, USA

[2]Jet Propulsion Laboratory, California Institute of Technology, Pasadena, CA, USA

[3]Institute of Geophysics, Department of Earth Sciences, ETH Zürich, Zürich, Switzerland

Contents of this file

Introduction This supporting information contains a more detailed description of the topographic evolution of the reference model.

Corresponding author: A. C. Adams, Institute of Geophysics and Planetary Physics, Scripps Institution of Oceanography, University of California, San Diego, CA, USA. (aca009@ucsd.edu)

Text S1.

Surface topography evolution was plotted in Supplementary Fig. 1 (A-E) over a section of the domain for the reference model. All delamination models exhibited similar changes in topographic features. For each model, we tracked the height and location of the forebulge and the depth and location of the trench over time. Initially, there was a topographic high over the surface of the gap as is expected due to the density contrast with adjacent lithosphere. Early in the model evolution (0.2 Myr), the edge of the thickest plate h_L bent downward into the mantle, creating a small trench (Supplementary Fig. 1A). As the slab continued to sink, a topographic low formed in association with the location of the trench and a topographic high formed on the surface of the down-going plate over the flexural bulge. The peak over the forebulge increased in height as both the forebulge and trench retreated steadily away from the initial gap zone (Supplementary Fig. 1B-D). The topography over the gap decreased in height compared to the initial stages and remained near zero elevation for the duration of the model evolution. A topographic high marked the edge of the non-delaminating plate with thickness h_{L-min}. The end of steady-state delamination was punctuated by the start of slab break-off at the surface. As the plate began to break-off at the surface, the magnitude of the trench depth and forebulge height decreased sharply. The trench and forebulge movement also suddenly changed directions from moving away from the gap to being pulled back toward the site of break-off. The timings of these changes in trench depth, forebulge height, and forebulge location were used to define the end of steady-state delamination for each model (see Fig. 9).

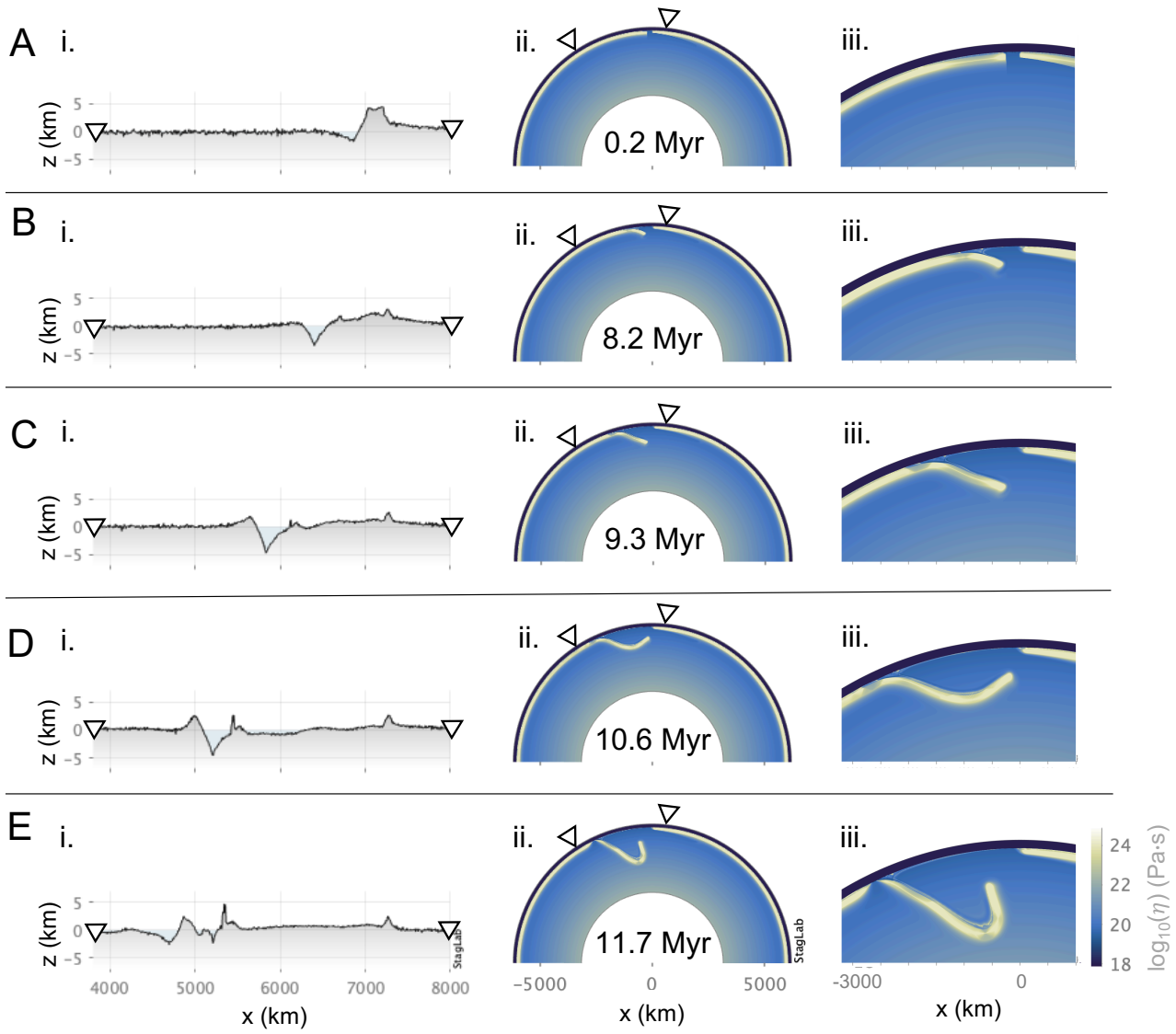

Figure S1. Typical evolution of a peel-back delamination event shown in the (i) topography field, (ii) global viscosity field, and (iii) local viscosity field of the reference model (B_{crust} = -300 kg/m^3, h_L = 250 km, η_{max} = 10^{24} Pa·s). Timing of model stages (A-E) correspond to Figure 5.